

INFRARED STUDIES OF ELLIPTICAL GALAXIES. I. AN OPTICALLY SELECTED SAMPLE

C. D. IMPEY^{1, 2, 3}

Astronomy Department, California Institute of Technology

AND

C. G. WYNN-WILLIAMS^{1, 2, 3} AND E. E. BECKLIN^{1, 2}

Institute for Astronomy, University of Hawaii

Received 1985 October 11; accepted 1986 March 28

ABSTRACT

The nuclei of 65 elliptical galaxies have been observed in the infrared, including the first large set of sensitive measurements of ellipticals at 10 μm . One-third of the sample is detected at greater than a 2σ level, and a null experiment of sky measurements is used to confirm the significance of the weak 10 μm signals. Near-infrared measurements of $\frac{2}{3}$ of the sample through a similar aperture are used to define the energy distribution of the nuclei from 1 to 10 μm . Photospheric emission from the dominant late-type giant population cannot account for the observed 10 μm flux in most galaxies; near-infrared data show that there is an excess above photospheric emission which is steep and contributes weakly at short wavelengths. It is unlikely that the steep infrared component represents the tail of the luminosity function of blazars, but we cannot rule out low luminosity and ubiquitous analogs of the radio-quiet quasars. The excess is unlikely to be generated in active star-forming regions.

Multiperture photometry of the nearby elliptical M32 is also presented. In this important test case, the 10 μm emission shows an excess above the flux predicted for giant photospheres, and the radial distributions of excess 10 μm and 2 μm light are similar. The infrared data for the whole sample is closely matched by a mixture of giants similar to that found in the galactic nuclear bulge and in the galactic disk. The nuclear colors indicate a population with metallicity at least twice the solar value. Cool and luminous M giants in these populations generate mass loss and infrared emission from circumstellar envelopes, and they contribute only a small fraction of the optical light in the galaxy. The very large 10 μm excesses seen in NGC 1052 and NGC 838 are probably not primarily the result of luminous M giants. There are at least two sources of 10 μm radiation in elliptical galaxies.

Subject headings: galaxies: nuclei — galaxies: photometry — galaxies: stellar content — infrared: sources

I. INTRODUCTION

The important stellar populations in elliptical galaxies have been known for over 30 yr, and the contribution of late-type giants to the optical light is well established (Stebbins and Whitford 1948; Whitford 1976). In the last few years, a series of 1–3 μm surveys of early-type galaxies have carefully defined the stellar populations and have put strong constraints on models by Tinsley and Gunn (1976), O'Connell (1976), and others. The importance of M giants to the stellar mix is established by the visual and near-infrared colors (Frogel *et al.* 1978), the TiO/Ca II band in the optical spectrum (O'Connell 1976), and the near-infrared bands at 2.29 μm (CO) and 1.9 μm (H_2O) (Frogel *et al.* 1975; Aaronson *et al.* 1978). These indices rule out large contributions to the infrared flux from dwarfs, and point to populations with $M/L \approx 5$ and a slope of the initial mass function (IMF) of $x \approx 1$, where $dN/dm \propto m^{-(1+x)}$ (Tinsley 1972). In terms of stellar evolution, the prevailing view

of elliptical galaxies is one of a single coeval stellar population of age ~ 15 Gyr with no subsequent bursts of star formation.

Recent observations have begun to complicate this simple view of ellipticals. Most galaxy models have difficulty in matching *both* the ultraviolet and infrared colors; there seems to be a missing component which is either very hot or cool and luminous (Aaronson 1981). Therefore, the question of recent or current star formation in ellipticals deserves careful attention. In general, ellipticals do not show the large aggregations of dust, gas, and young massive stars that are characteristic of current star formation (Faber and Gallagher 1976; Knapp, Turner, and Cunniffe 1985; van den Bergh 1975). From his search for hot stars in ellipticals, Rose (1986) has put a limit of 4% on the fraction of 4000 Å light that can come from stars formed in the last Gyr. The H I limits ($10^8 M_\odot$) even rule out episodic star formation because the burst decay time is long relative to the interval between bursts, and the gas mass would rise above the detectable limit. The few exceptions are generally galaxies with obvious morphological peculiarities (e.g., Cen A and NGC 205).

On the other hand, there is evidence for a hot component from *IUE* observations of some galaxies (Bertola and Oke 1982) and the spectra fitting of Gunn, Stryker, and Tinsley (1981). Renzini (1981) has suggested that the hot component is a post-asymptotic giant branch stage, which provides only $\sim 1\%$ of the *V* light but peaks strongly below 2000 Å. It is difficult to rule out star formation entirely, since we have no

¹ Visiting Astronomer, NASA Infrared Telescope Facility (IRTF), which is operated by the University of Hawaii under contract from the National Aeronautics and Space Administration.

² Visiting Astronomer, United Kingdom Infrared Telescope (UKIRT), which is operated by the Royal Observatory for the British Science and Engineering Research Council

³ Visiting Astronomer, National Radio Astronomy Observatory, which is operated by Associated Universities, Inc., under contract with the National Science Foundation.

a priori knowledge of the IMF, and large numbers of low-mass, low-luminosity stars may be forming. Evidence in this direction comes from Forman, Jones, and Tucker (1985), who detected hot gaseous X-ray coronae in a number of ellipticals. They conclude from the X-ray data that the values of the gas mass and star formation rate in luminous ellipticals can be similar to the values in our own Galaxy. The general absence of patchy obscuration, large dusty areas, H II regions, and anomalous ultraviolet colors is only evidence against the formation of massive stars.

The limits on *current* star formation in ellipticals are quite strong, but there is some evidence for *previous* star formation in the form of an intermediate age population (5–10 Gyr). O'Connell (1980) has presented convincing evidence for a 5×10^9 yr old population of stars in M32. Also, both Rose (1986) and Burstein *et al.* (1984) have discussed widespread but subtle differences between the spectra of elliptical galaxies and metal-rich galactic globular clusters. The differences may be most plausibly explained by an intermediate age population in elliptical galaxies. We note that if star formation is to mop up the mass loss from the late phases of giant evolution, it must be very efficient and it must also be widespread throughout the galaxies. Therefore, the effects of previous generations of star formation should be seen beyond the nucleus of the galaxy. The subject of stellar populations in galaxies has been confused by the nonuniqueness of synthesis models and the fact that the ultraviolet and infrared spectral regions are dominated by small populations of luminous, rapidly evolving stars. It is likely that many of the discrepancies between the models and observations will be removed by including stars with a realistic range of metal abundances.

The nuclear colors of an elliptical can also be altered by nonthermal activity. There is a range of nuclear radio activity in ellipticals ranging from luminous 3CR radio sources to nearby weak BL Lac objects. Recently, there has been a surge of interest in the low-luminosity tail of the nuclear activity spectrum (Balick and Heckman 1983). However, the radio luminosity function for ellipticals indicates that weak core activity is rare (Meier *et al.* 1979; Hummel, Kotanyi, and Ekers 1985). Only *compact* radio activity is expected to appear as an infrared core component, since the galaxy counterparts to the *extended* 3CR sources have normal stellar colors (Lilly and Longair 1982). In a search for either inactive nuclei or active star forming regions, the most effective wavelength region is the infrared. The energy distribution of the dominant giant population peaks at $1.5 \mu\text{m}$, and by $10 \mu\text{m}$ the photospheric flux is falling rapidly. By contrast, the contribution of a non-thermal power law or a cool thermal source rises into the far-infrared.

Only a few investigations of elliptical galaxies at wavelengths longer than $3 \mu\text{m}$ have been published (Rieke and Low 1972; Becklin, Tokunaga, and Wynn-Williams 1982; Rieke, Lebofsky, and Kemp 1982; Puschell 1981*a, b*). In the radio galaxies studied by Puschell, the excess over photospheric emission has been interpreted as dust emission in the nucleus; but in NGC 1052, there is disagreement over whether the infrared emission is due to thermally radiating dust or the presence of a miniblazar. The recent results of the successful *IRAS* satellite have added little to our knowledge of the infrared properties of ellipticals because relatively few have been detected. A paper by Habing *et al.* (1984) contains fluxes for M32, NGC 205, and the nucleus of M31 (presumed to be relatively gas- and dust-free), but none of the other galaxy or

cluster observations have been successful at detecting ellipticals (Rowan-Robinson *et al.* 1984; de Jong *et al.* 1984; Soifer *et al.* 1984; Young *et al.* 1984). Since the 1σ rms sensitivity of our $10 \mu\text{m}$ observations is a factor of 9 fainter than the Band 1 ($12 \mu\text{m}$) 1σ sensitivity of the *IRAS* survey, the paucity of *IRAS* ellipticals is not surprising. More may be detected in pointed observations and coadded survey data which reach 3 or 4 times deeper than the survey limit. The galaxies from our sample which are included in the *IRAS Point Source Catalog* are discussed later in the paper. In this paper, we greatly enlarge the sample of ellipticals that has been observed at $10 \mu\text{m}$.

II. THE SAMPLE

A total of 65 galaxies were observed at $10 \mu\text{m}$, and 47 of these were also observed in the $1\text{--}3 \mu\text{m}$ region. A majority of the ellipticals are bright galaxies from optical catalogs which have also been searched for radio emission. Optical data for all these galaxies are published in de Vaucouleurs, de Vaucouleurs and Corwin (1976, hereafter RC2). Sixty of the galaxies are also included in the revised *Shapley-Ames Catalogue* (Sandage and Tammann 1981). Since the Shapley-Ames is essentially complete down to $B_T = 12.7$ and contains 173 E or E/S0 galaxies, our sample observed in the infrared contains a large proportion of the brightest ellipticals in the sky. Most of the sample has been surveyed for radio emission by Dressel and Condon (1978) at Arecibo or by Hummel (1980) at Westerbork with detection limits of 15 mJy (2380 MHz) and 10 mJy (1400 MHz), respectively. Additional radio measurements are in Disney and Wall (1977), and Hummel, Kotanyi, and Ekers (1985). Recently, we have surveyed all 65 galaxies for 6 cm radio emission, with the result that over 60% are now detected. In this paper, we incorporate our improved radio detection limits of ~ 1 mJy. In a companion paper, we discuss infrared observations of 43 *radio-selected* elliptical galaxies (Impey, Wynn-Williams, and Becklin 1986).

III. INFRARED OBSERVATIONS

a) 10 Micron Observations

The main aim of this project was a comprehensive study of elliptical galaxies at $10 \mu\text{m}$. All of the infrared observations were made between 1982 September and 1983 September with the 3 m NASA Infrared Telescope Facility located on Mauna Kea in Hawaii (IRTF)⁴. A gallium-doped germanium bolometer was used at the Cassegrain focus with a $5''.7$ circular entrance aperture and a broad-band $8\text{--}13 \mu\text{m}$ filter. Secondary chopping at a rate of 13 Hz and an amplitude of either $10''$ or $20''$ was used, giving good cancellation of possible extended emission. Flux calibration was carried out by measuring β And, α Tau, β Gem, α Boo, α Lyr, and β Peg, for which the fluxes at an effective wavelength of $10.2 \mu\text{m}$ were assumed to be 249, 581, 104, 673, 37, and 387 Jy. Beam profiles recorded every run showed the instrument response to be uniform and symmetric, with a beam width at half-power of $5''.5$.

The 65 galaxies were measured on 10 separate nights during 1982 September and 1983 January, February, March, and September. The $10 \mu\text{m}$ measurements for seven galaxies were repeated on more than one night. Most of the $10 \mu\text{m}$ data was taken during exceptionally dry and clear runs in 1982 September and 1983 February. Galaxies were acquired by centering

⁴ The Infrared Telescope Facility is operated by the University of Hawaii under contract from the National Space and Aeronautics Administration.

TABLE 1
10 MICRON AND RADIO DATA

Galaxy (1)	Hubble Type (2)	Velocity ^a (km s ⁻¹) (3)	Observation Date (UT) (m/d/y) (4)	GHz Flux ^b (mJy) (5)	10 μm Flux (mJy) (6)	10 μm Noise (mJy) (7)	Notes ^c (8)
NGC 147 (DDO 3)	dE5	252	9/18/82	12	4.0	7.4	H
NGC 205	E5 pec	-239	9/19/82	<1	-3.4	6.1	I
			9/05/83	...	4.4	10.9	
NGC 221 (M32)	E2	-217	9/19/82	<1	63.6	5.7	I, *
			1/01/85	...	61.0	10.0	*
NGC 547	E1	5378	9/05/83	(408)	6.1	5.6	H
NGC 584 (PKS)	S0	1811	9/20/82	<1	14.0	6.1	*
			9/05/83	...	11.1	8.7	
NGC 596	E0 pec	2049	9/20/82	<1	16.5	7.3	*
			9/05/83	...	1.4	7.6	
NGC 636	E1	1941	9/20/82	6	5.8	6.4	
NGC 720	E5	1808	9/20/82	<1	4.6	5.5	
NGC 741 (4C 05.10)	E0	5559	9/20/82	(441)	4.0	7.6	H
NGC 750 (VV 189)	E0 pec	5126	9/19/82	<1	0.2	7.6	
NGC 777	E1	4995	9/20/82	12	8.1	6.9	
NGC 838	I0 pec	3870	9/05/83	(45)	72.5	5.9	DW, I, *
NGC 1052 (PKS)	E3/S0	1439	9/19/82	(560)	117.6	11.3	H, I, *
NGC 1199	E3	2531	9/05/83	<1	3.2	8.3	
NGC 1209	E6	2563	9/20/82	12	3.3	6.6	
			9/05/83	...	4.1	7.8	
NGC 1395	E2	1691	9/19/82	2	20.2	7.3	*
NGC 1407	E0	1811	9/19/82	(50)	4.3	7.2	H
NGC 1426	E4	1358	9/05/83	<1	6.7	5.9	
NGC 1587	E1 pec	3890	9/20/82	(87)	13.4	5.8	DC, *
NGC 2693	E2	4956	2/10/83	2	18.4	7.0	*
NGC 2768	E6/S0	1408	2/10/83	(13)	2.5	8.7	H
NGC 3158	E3	7024	2/09/83	3	3.4	8.7	
NGC 3377	E6	718	2/09/83	<1	0.0	7.8	
NGC 3379 (M105)	E0	885	2/10/83	2	15.0	7.2	*
NGC 3610	E5	1765	2/09/83	5	16.1	7.8	*
NGC 3613	E6	2054	2/09/83	<1	13.7	8.4	
NGC 3640	E2	1354	2/10/83	4	2.8	6.3	
NGC 4125	E6 pec	1339	2/10/83	3	-10.0	9.2	I
NGC 4168	E2	2307	3/16/83	4	-3.0	7.5	
NGC 4261 (3C 270)	E3	2202	2/08/83	(210)	29.9	7.7	H, *
NGC 4278 (B2)	E1	659	2/08/83	(480)	18.5	8.4	H, I, *
NGC 4342 (IC 3256)	E7	1170	3/16/83	5	4.3	8.3	
NGC 4365	E3	1177	2/09/83	<1	0.0	7.5	
NGC 4374 (M84)	E1	933	2/09/83	(3635)	20.9	7.2	H, I, *
NGC 4406 (M86)	E3/S0	-225	2/09/83	<1	7.0	6.4	I
NGC 4472 (M49)	E1/S0	914	2/09/83	250	7.5	6.1	
NGC 4473	E5	2279	2/10/83	<1	19.7	5.8	*
NGC 4476	E5 pec	1978	3/16/83	<1	9.3	8.9	I
NGC 4478	E2	1482	3/16/83	(2200)	9.7	8.1	H
NGC 4486 (M87)	E0	1257	2/09/83	(1000)	34.6	6.2	H, I, *
NGC 4494	E1	1307	2/10/83	1	9.7	10.4	
NGC 4550	E7/S0	350	3/16/83	<1	25.1	12.3	*
NGC 4552 (M89)	E0/S0	239	2/09/83	(62)	21.1	7.6	H, *
NGC 4564	E6	1020	3/16/83	<1	20.0	8.6	*
NGC 4621 (M59)	E5	414	2/09/83	6	8.0	6.1	
NGC 4623	E7	1788	3/16/83	2	3.2	8.7	
NGC 4636	E0/S0	979	2/09/83	(47)	-6.2	5.8	H
NGC 4649 (M60)	E2/S0	1200	2/10/83	(25)	-11.2	9.3	H
NGC 4660	E5	1017	3/16/83	<1	17.9	8.9	*
NGC 4697	E6	1308	2/10/83	<1	25.2	7.5	*
NGC 4880	E4/S0	1419	3/16/83	<1	24.0	11.5	*
NGC 5018	E4	2897	2/10/83	3	5.8	8.7	I
NGC 5322	E4	1902	2/10/83	(87)	14.4	9.2	H
NGC 5557	E2	3293	2/10/83	<1	22.9	9.4	*
NGC 5576	E4	1528	2/10/83	<1	6.5	10.9	
NGC 5813	E1	1882	9/07/83	5	-2.4	10.5	
NGC 5846	E0/S0	1713	2/10/83	(17)	0.5	10.5	H
NGC 5982	E3	2879	2/10/83	<1	8.9	10.5	
NGC 6047	S0	9470	9/20/82	175	5.1	7.3	
NGC 6454	E	9120	9/19/82	210	-6.0	7.0	
NGC 6482	E2	3922	9/20/82	13	8.8	8.5	
NGC 6702	E3	4725	9/05/83	<1	0.2	9.1	
			9/07/83	...	1.0	11.5	
NGC 7385	E1 pec	7827	9/19/82	(1135)	7.7	8.0	H
NGC 7507	E0	1637	9/18/82	<1	14.2	7.7	
			9/07/83	...	13.9	11.1	
NGC 7728	E2	9472	9/19/82	(390)	3.8	6.7	H

^a Velocities from RC2.

^b Radio limits are 5 σ.

^c NOTES.—* denotes ≥ 2 σ number. I denotes IRAS detection. H, DW, DC are radio fluxes from Hummel 1980, Disney and Wall 1977, and Dressel and Condon 1978, respectively.

the aperture on the optical nucleus using the Quantex TV camera. In order to cover a large number of galaxies down to a uniform sensitivity limit, an integration time of 20 minutes was chosen for each galaxy. Measurement statistics calculated from the 60 left-right pairs of each integration showed an average noise sensitivity of 7.8 mJy. This experiment is roughly twice as deep as the survey of Virgo spirals published by Scoville *et al.* (1983).

At the start of the project, it was apparent that many of the ellipticals were registering small but positive 10 μm fluxes. To check for instrumental bias, we began a sequence of sky measurements with the same integration time as the galaxy measurements. The procedure was simply to move off a galaxy onto a patch of sky that was blank down to the limit of the Palomar Sky Survey, and integrate with the instrument (gain, chopper throw, chopper frequency) unchanged. Sky measurements were made every night, interspersed between galaxy measurements. A total of 27 measurements were made in this way. This subsidiary experiment provides a very fine check on any signal bias in the bolometer, chopper and telescope system as well as providing a check on sky emission. The 10 μm fluxes are listed in Table 1. Columns (1)–(7) contain the galaxy NGC number (and other names), Hubble type (Sandage and Tammann 1981), velocity (km s^{-1}), date of observation, radio flux in mJy, 10 μm flux, and measurement noise. Notes are given in column (8) and explained in a footnote. Galaxies having a flux with significance greater than 2σ are marked with an asterisk. Galaxies with a detection in the *IRAS Point Source Catalog* have the letter *I* in the final column of Table 1. The fluxes have not been corrected for the bandwidth of the 10 μm filter; this effect is at most 10%. No extinction corrections have been applied, since they would be much smaller than the statistical errors. No bias is introduced by neglecting an extinction correction.

b) Near-Infrared Observations

To supplement the 10 μm data, we obtained 1–4 μm photometry for many of the ellipticals in the sample. The 47 galaxies measured at short wavelengths are typical of the larger 10 μm sample in terms of the distributions of 10 μm flux, Hubble type, and distance. We will therefore assume that the near-infrared properties derived from this subset are representative of the entire sample. An indium antimonide (InSb) detector cooled by solid nitrogen was used at the Cassegrain foci of both the IRTF and the 3.8 m United Kingdom Infrared Telescope (UKIRT)⁵ on Mauna Kea. The apertures used were 5".8 (IRTF) and 7".5 (UKIRT) in diameter. The data were acquired during the periods 1983 September 2–6 (IRTF) and 1984 March 23–26 (UKIRT). NGC 1052 was not observed during these runs, and near-infrared data from Becklin, Tokunaga, and Wynn-Williams are reproduced in Table 2. The effective wavelengths and bandwidths of the filters were: *J* (1.25, 0.30 μm), *H* (1.65, 0.35 μm), *K* (2.20, 0.42 μm), and *L* (3.80, 0.67 μm). Observations at all wavelengths were made through similar sized apertures, and identical filter sets were used on both the IRTF and UKIRT. Flux standards from the list of Elias *et al.* (1982) were observed at the beginning, middle, and end of each night. The accuracy of the repeated standard measurements was $\sim 2\%$, which generally dominates the statistical errors of under 1% (except in the *L* band). The errors for the magnitudes, dictated

by the rms deviation of the standard star measurements, are 0.02 mag at *J*, *H*, and *K*, and the mean photometric error is 0.07 mag at *L*. In general, the colors will be more accurate than the absolute flux densities because the different filter measurements were made in close succession, and most of the corrections that have been applied to the data have only a weak color dependence. Flux density in absolute units was calculated by assuming the monochromatic flux from a zero magnitude star to be 1520 Jy at *J* (1.25 μm), 980 Jy at *H* (1.65 μm), 620 Jy at *K* (2.2 μm), and 230 Jy at *L* (3.8 μm). Galaxies were acquired by centering the aperture on the optical nucleus using the Quantex TV camera, and in each case this procedure was checked by peaking up automatically on the 1.65 μm signal. Table 2 gives the details of the near-infrared data, with the galaxy NGC number and the ratio of aperture size to galaxy diameter, $\log A/D(0)$, in columns (1) and (2). Following the somewhat eccentric units of de Vaucouleurs, de Vaucouleurs, and Corwin (1976), $\log A/D(0)$ is the decimal logarithm of the ratio of the aperture to the effective diameter in units of 0.1. The galaxy magnitudes at *J*, *H*, *K*, and *L*, corrected only for atmospheric extinction, are given in columns (3), (5), (7), and (9). The colors in columns (4), (6), and (8) have been corrected for a series of effects described below, including color terms to transform the data from the IRTF to the CTIO/CIT system. This transformation is carried out to simplify the comparison of this data set with previous results on ellipticals and late type giants.

All the data have been corrected for atmospheric extinction with coefficients derived from each night of observation. The instrument response function was determined by drifting a point source across the aperture in each filter, and the resulting beam profiles were flat-topped and symmetric with a full width at half-power of 5".8 (IRTF). The corresponding full width on UKIRT was 7".5. Convolution of the beam profile with a typical elliptical galaxy profile showed that there are corrections to the galaxy flux density due to the shape of the beam sensitivity profile. These corrections of typically 1%–2% were not applied since they are less than the photometric errors. For nearby galaxies, *K*-corrections are generally small and linear in redshift; for *z* of up to 0.03 the corrections of Frogel *et al.* (1978) were adopted, i.e., $\Delta J = -0.7z$, $\Delta H = -0.2z$, $\Delta K = 3.3z$, $\Delta L = 3.5z$. Corrections for interstellar reddening were made using the H II column density tabulation of Burstein and Heiles (1982). The H I column density for each galaxy was scaled to $2.3 \times 10^{21} N_{\text{H}} = 1.0 \text{ mag } A_V$. Selective extinction coefficients were taken from O'Dell *et al.* (1978): $A_J/A_V = 0.23$, $A_H/A_V = 0.13$, $A_K/A_V = 0.09$, $A_L/A_V = 0.05$ (this assumes $A_V/E_{B-V} = 3.1$). We note that for $A_V \leq 0.10$, near-infrared extinction is negligible, and the largest corrections applied were 2%–3% at the shortest wavelengths.

Since the galaxies subtend large angles on the sky, a small correction for galaxy flux in the reference beam must be applied. The size of this upward correction to the flux depends on the throw of the chopper and the value of $\log A/D(0)$ for the galaxy, the ratio of aperture size to corrected isophotal diameter (taken from RC2). We use the curve of growth of Frogel *et al.* (1978) and extend it to smaller values of $\log A/D(0)$, since it does not cover the range appropriate to these small aperture measurements. The values of $\log A/D(0)$ and \log of the flux decrement are: $\log A/D(0) = -0.9$, $\Delta \log S_K = -0.2$; $\log A/D(0) = -1.2$, $\Delta \log S_K = -0.45$; $\log A/D(0) = -1.5$, $\Delta \log S_K = -0.75$; $\log A/D(0) = -1.8$, $\Delta \log S_K = -1.28$. The error in this curve is about ± 0.15 in $\Delta \log S_K$. A different

⁵ The United Kingdom Infrared Telescope is operated by the Royal Observatory Edinburgh for the British Science and Engineering Research Council.

TABLE 2
NEAR-INFRARED DATA

Galaxy ^a (1)	$\log A/D(0)^b$ (2)	J^c (3)	$(J-H)_c$ (4)	H (5)	$(H-K)_c$ (6)	K (7)	$(K-L)_c$ (8)	L (9)
NGC 205	-2.18	13.11	(0.67)	12.37	(0.14)	12.22	(0.50)	11.71
NGC 221	-1.86	8.88	(0.69)	8.12	(0.16)	7.95	(0.18)	7.76
NGC 547	-1.23	12.20	(0.76)	11.38	(0.20)	11.11	(0.24)	10.87
NGC 584	-1.53	10.87	(0.78)	10.03	(0.20)	9.81	(0.28)	9.53
NGC 596	-1.49	11.32	(0.77)	10.49	(0.17)	10.29	(0.26)	10.01
NGC 636	-1.35	11.51	(0.78)	10.67	(0.17)	10.47	(0.21)	10.27
NGC 720	-1.59	11.44	(0.80)	10.57	(0.19)	10.36	(0.26)	10.11
NGC 741	-1.51	12.23	(0.76)	11.39	(0.20)	11.12	(0.17)	10.96
NGC 750	-1.42	12.61	(0.74)	11.80	(0.19)	11.53	(0.20)	11.33
NGC 838	-1.23	12.41	(0.79)	11.55	(0.29)	11.20	(0.85)	10.35
NGC 1052	-1.42	10.78	(0.71)	10.02	(0.30)	9.72	(0.53)	9.25
NGC 1199	-1.33	11.73	(0.77)	10.89	(0.19)	10.68	(0.20)	10.48
NGC 1209	-1.36	11.43	(0.70)	10.67	(0.18)	10.42	(0.29)	10.13
NGC 1395	-1.48	11.13	(0.81)	10.25	(0.17)	10.06	(0.28)	9.88
NGC 1407	-1.39	11.44	(0.78)	10.57	(0.19)	10.36	(0.29)	10.06
NGC 1426	-1.29	11.81	(0.72)	11.04	(0.19)	10.83	(0.19)	10.64
NGC 1587	-1.31	11.75	(0.79)	10.87	(0.17)	10.64	(0.27)	10.36
NGC 2693	-1.19	11.54	(0.73)	10.74	(0.21)	10.46	(0.22)	10.24
NGC 3158	-1.24	11.87	(0.71)	11.10	(0.23)	10.79	(0.41)	10.37
NGC 3377	-1.47	10.49	(0.67)	9.77	(0.23)	9.53	(0.32)	9.22
NGC 3379	-1.52	9.94	(0.73)	9.16	(0.24)	8.91	(0.27)	8.64
NGC 3640	-1.47	10.94	(0.68)	10.19	(0.24)	9.95	(0.31)	9.63
NGC 4261	-1.54	10.98	(0.70)	10.23	(0.23)	10.00	(0.36)	9.64
NGC 4278	-1.43	10.36	(0.73)	9.58	(0.20)	9.38	(0.28)	9.10
NGC 4365	-1.64	10.67	(0.71)	9.91	(0.23)	9.68	(0.39)	9.29
NGC 4374	-1.57	10.20	(0.77)	9.37	(0.19)	9.18	(0.33)	8.85
NGC 4406	-1.72	10.57	(0.70)	9.82	(0.21)	9.61	(0.32)	9.29
NGC 4472	-1.81	10.25	(0.73)	9.47	(0.22)	9.25	(0.35)	8.90
NGC 4473	-1.47	10.35	(0.69)	9.60	(0.22)	9.36	(0.28)	9.07
NGC 4486	-1.74	10.93	(0.74)	10.19	(0.24)	9.95	(0.49)	9.47
NGC 4494	-1.53	10.56	(0.73)	9.78	(0.22)	9.56	(0.34)	9.23
NGC 4552	-1.50	10.09	(0.75)	9.28	(0.23)	9.05	(0.30)	8.76
NGC 4621	-1.54	10.09	(0.73)	9.30	(0.24)	9.06	(0.29)	8.77
NGC 4636	-1.65	11.01	(0.73)	10.21	(0.21)	9.99	(0.32)	9.66
NGC 4649	-1.73	10.23	(0.77)	9.40	(0.24)	9.16	(0.31)	8.85
NGC 4697	-1.73	10.30	(0.73)	9.52	(0.26)	9.26	(0.29)	8.97
NGC 5018	-1.28	10.59	(0.70)	9.82	(0.28)	9.51	(0.42)	9.13
NGC 5557	-1.26	11.20	(0.74)	10.39	(0.19)	10.16	(0.32)	9.84
NGC 5576	-1.34	10.63	(0.70)	9.88	(0.20)	9.66	(0.31)	9.36
NGC 5982	-1.44	11.45	(0.80)	10.58	(0.16)	10.38	(0.27)	10.10
NGC 6047	-1.10	13.52	(0.83)	12.61	(0.15)	12.36	(0.50)	11.86
NGC 6454	-1.13	12.57	(0.79)	11.70	(0.16)	11.44	(0.31)	11.13
NGC 6482	-1.36	11.70	(0.78)	10.82	(0.17)	10.58	(0.24)	10.33
NGC 6702	-1.30	12.23	(0.74)	11.41	(0.11)	11.23	(0.29)	10.94
NGC 7385	-1.19	12.72	(0.81)	11.83	(0.17)	11.56	(0.24)	11.31
NGC 7507	-1.42	10.85	(0.85)	9.93	(0.17)	9.74	(0.25)	9.49
NGC 7728	-1.08	12.51	(0.82)	11.61	(0.18)	11.31	(0.29)	11.02

^a Colors include various corrections discussed in § IIIb.

^b Values of $\log A/D(0)$ from RC2.

^c Fluxes measured in 7.5 aperture.

locus of corrections is calculated for each different beam throw. Chopper throw corrections are not included in the Table 2 flux densities. The median value of the reference beam correction is 7%, and is somewhat higher for the few measurements of larger galaxies or using smaller beam throws. Since color gradients in ellipticals are small ($\Delta J-K \leq 0.04$, $-1.2 < \log A/D(0) < -0.3$), the correction is the same for all wavebands and the accuracy of the near-infrared colors is not affected.

The equivalent monochromatic fluxes are not modified by a bandwidth correction, because in all cases it is $\leq 1\%$. However, there is a color term that must be applied to the IRTF colors, to transform between the IRTF and the CTIO/CIT (Elias *et al.* 1982) systems. A. L. Longmore and P. M. Williams (1985, private communication) have determined color equations based on 21 primary and 28 secondary standards,

with zero points coming from a forced fit to the blue stars in Elias *et al.* (1982) and Allen and Cragg (1982). The adopted equations are $(J-H)_{\text{IRTF}} = 1.07 (J-H)_c$ and $(K-L)_{\text{IRTF}} = 1.12 (K-L)_c$. There is no color term in the K filter. The present measurements use the L filter rather than the original Johnson L filter because L is a narrower window, has a cleaner atmospheric window with less extinction, and offers a slightly longer wavelength baseline. To compare with published measurements using the L filter, we note that for mean elliptical colors $(K-L)_c = 1.14 (K-L)_c + 0.09$.

c) M32 Observations

NGC 221, commonly referred to as M32, is a satellite of M31 in the Local Group. It is also one of the few galaxies in the sky close enough that the photospheric emission from giant

stars should readily be detected at $10\ \mu\text{m}$. Because of this, additional multiaperture measurements were made on the IRTF on 1984 December 31 employing the same instrument and reduction procedures used for the bulk of the data in this paper. The multiaperture data were taken using a relatively large beam separation of $30''$, so a reference beam correction has not been applied. The standard IRTF bolometer was used for both the $2\ \mu\text{m}$ and $10\ \mu\text{m}$ measurements. Photometry in three different apertures at $2\ \mu\text{m}$ and $10\ \mu\text{m}$ gave the following results: $3''8$: $S_K = 253\ \text{mJy}$, $S_N = 23 \pm 7\ \text{mJy}$; $5''7$: $S_K = 416\ \text{mJy}$, $S_N = 61 \pm 10\ \text{mJy}$; $7''6$: $S_K = 565\ \text{mJy}$, $S_N = 66 \pm 10\ \text{mJy}$. Fluxes at $2.2\ \mu\text{m}$ have errors of $\sim 3\%$. The new multiaperture results show that the $2\ \mu\text{m}$ and $10\ \mu\text{m}$ radiation scale similarly with radius in M32.

d) Radio Observations

Since only one-third of the galaxies in our sample had been detected by previous radio measurements, 6 cm observations were made with the Very Large Array⁶ to improve the detection rate. The ellipticals were observed using 20 antennas of the C array configuration on 1984 June 2-3. Each observation

⁶ The National Radio Astronomy Observatory is operated by Associated Universities, Inc., under contract with the National Science Foundation.

consisted of 10 minutes' integration in snapshot mode, giving an average rms sensitivity of $0.2\ \text{mJy}$. Standard calibration and reduction procedures were used, with natural weighting of the UV data for maximum sensitivity to weak point sources. The new data doubled the detection rate in this sample to 60% and improved the upper limits for the remaining galaxies by an order of magnitude. Radio data for the 65 ellipticals is presented in column (5) of Table 1. New detections and $5\ \sigma$ upper limits at 6 cm are shown in units of mJy, with previous data from Hummel (1980) at 1400 MHz, Disney and Wall (1977) at 4985 MHz, and Dressel and Condon (1978) at 2380 MHz included in parentheses. The interpretation of the full VLA data set, and a discussion of the radio luminosity function for ellipticals, will be presented in a future paper.

IV. RESULTS

a) Faint 10 Micron Sources

The histogram of $10\ \mu\text{m}$ fluxes is shown in Figure 1a, together with the expected measurement noise distribution (a Gaussian with $\sigma = 7.8\ \text{mJy}$). Figure 1b shows a similar histogram for the 27 sky measurements. The measurements with asterisks in Table 1 have a significance of $2\ \sigma$ or greater; one-third of the sample (22 out of 65) fall into this group. It will be

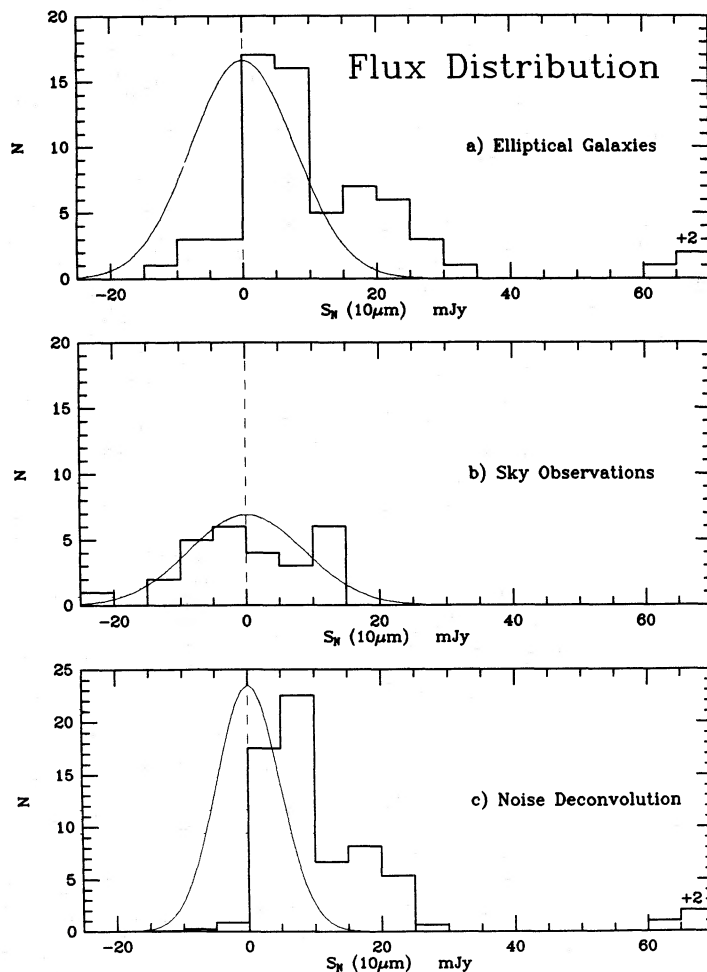


FIG. 1.—(a) Galaxy $10\ \mu\text{m}$ flux distribution with noise distribution of rms $7.8\ \text{mJy}$ superposed. (b) Sky $10\ \mu\text{m}$ flux distribution with noise distribution superposed. (c) Histogram of galaxy fluxes after Lucy noise deconvolution.

demonstrated that essentially all of these galaxies are true detections. Figure 1a also shows a strong positive bias, above that expected by the noise distribution or measured by the sky distribution. Although many of the individual galaxies have a low level of significance, the ensemble indicates that a low level of $10\ \mu\text{m}$ emission is present. Measurements of low signal-to-noise ratio are generally suspect in astronomy, because there are so many effects that can invalidate the Central Limit Theorem and make the normal distribution inapplicable. However, in this case we have *measured* the underlying noise distribution with the integrations on the sky. In this section, appropriate statistical tests are used to demonstrate what is apparent to the eye in Figure 1, that many of the galaxies have weak but real levels of $10\ \mu\text{m}$ emission. Each galaxy has a measurement noise calculated from 60 20 s samples. The mean amplitude of all the noise measurements is 7.8 mJy with a standard deviation of 1.5 mJy. This dispersion is small enough that a mean noise of 7.8 mJy will be used in all of the statistical tests (there is no correlation between the amplitude of noise and galaxy signal). The mean and standard deviation of 27 sky measures is 0.03 ± 9.6 mJy, showing no trace of the positive bias found for the galaxies.

Since many of the individual detections are very weak, the consistency and repeatability of the $10\ \mu\text{m}$ data must be tested. The comparison comes from two sources: repeat measures of eight galaxies listed in Table 1, and previous observations of seven galaxies at $10\ \mu\text{m}$ from the literature. The previous data were all collected through similar sized apertures and N filters by Rieke and Low (1972), Puschell (1981a), Rieke and Lebofsky (1978), and Becklin, Tokunaga, and Wynn-Williams (1982). We exclude M87 (NGC 4486) from the comparison because it is known to have an active nucleus which may be variable at infrared wavelengths. Another three galaxies have only upper limits published, but they are all consistent with the subsequent IRTF measurement. Of the remaining 11 pairs of observations, all agree to $\leq 1\ \sigma$. Overall, there is excellent statistical agreement with previous measurements.

i) Mann-Whitney Test

The Mann-Whitney U is a powerful nonparametric test for the comparison of two samples (Siegel 1956). Use of a nonparametric test is critical, since the aim is to *demonstrate* that the noise measures are drawn from a Normal Distribution. The null hypothesis is that the two samples are drawn from the same population. First, the distribution of sky observations is compared with the same number of normally distributed measurements with standard deviation 7.8 mJy. There is only a 30% ($0.4\ \sigma$) chance that the two samples are different, so the assumption of normally distributed errors for the sky and galaxy measurements is clearly a good one. On the other hand, when the galaxy distribution is compared with either the sky or noise distributions, the null hypothesis is rejected at better than the 99.9% significance level.

ii) The $P(\geq S_0)$ Statistic

We next construct a statistic to decide what *proportion* of galaxies have larger than a certain flux S_0 in the underlying flux distribution, when the substantial uncertainty of each measurement is accounted for. For each galaxy we can calculate the probability that the flux is greater than some threshold, $S \geq S_0$. By adding the probabilities for each galaxy and normalizing, the number of objects likely to have intrinsic fluxes greater than S_0 can be determined. As with the independent Mann-Whitney test, the $P(\geq S_0)$ statistic shows that the galaxy

and sky/noise flux distributions are different at better than the 99.9% significance level. Another use of the $P(\geq S_0)$ statistic is to test the reliability of the $2\ \sigma$ level of detection. Integrating the probabilities for the galaxies gives 20% of the sample with intrinsic flux $S \geq 15$ mJy. Since 21 out of 65 (32%) of the sample were measured at $\geq 2\ \sigma$, essentially all of these are real detections. It is also noted that none of the 27 sky observations resulted in a $\geq 2\ \sigma$ positive number.

iii) Lucy Noise Deconvolution

The iterative method described by Lucy (1974) can be used to detect weak signals in the presence of noise. When applied to the noise function, a Gaussian of half-width 7.8 mJy, the Lucy method gives as output a Gaussian of half-width 4.8 mJy. The power of the deconvolution is limited by the binsize of 5 mJy. The deconvolved flux distribution is shown in Figure 1c. After 10 iterations, 96% of the measurements are positive. Noise deconvolution shows that most of the ellipticals have real, positive $10\ \mu\text{m}$ fluxes.

b) Strong 10 Micron Sources

The three galaxies with fluxes greater than 40 mJy that lie beyond the main distribution of $10\ \mu\text{m}$ fluxes deserve special mention.

i) M32

The nearby dwarf elliptical M32 is a companion to M31 that has normal late-type stellar colors in the nucleus and a steep cusp in the central light distribution. The outer isophotes are smooth and symmetric, and apart from a tilt in the velocity dispersion curve it shows no evidence of interaction with M31. Dynamical studies point to a $5 \times 10^6 M_\odot$ mass concentration in the nucleus (Tonry 1984). The *IRAS Point Source Catalog* (PSC) only lists a detection of 0.39 Jy at $12\ \mu\text{m}$. However, pointed observations with the *IRAS* satellite (Habing *et al.* 1984) show that M31 has a similar $10\ \mu\text{m}$ to $20\ \mu\text{m}$ flux ratio to M32. Since both are relatively gas- and dust-free, M32 probably represents a good nearby datum on the mid-infrared properties of the late stellar component in ellipticals. The new multiaperture data for M32 are plotted in Figure 2, where the ratio of $2.2\ \mu\text{m}$ flux to $10\ \mu\text{m}$ flux is shown as a function of log aperture size. The *IRAS* data for M32 has been plotted on Figure 2. The Band 1 ($12\ \mu\text{m}$) flux from the PSC is 0.39 Jy, with an equivalent aperture diameter of $120''$ (2.65×10^{-7} sr from the *PSC Explanatory Supplement*). A color correction of 25% is used to increase the $12\ \mu\text{m}$ flux to an equivalent monochromatic $10\ \mu\text{m}$ flux. The $2.2\ \mu\text{m}$ flux of Frogel *et al.* (1978) is used, adjusted slightly from $111''$ aperture to $120''$ using their curve of growth. Within the errors the ratio of S_K/S_N is constant with radius, and the $2.2\ \mu\text{m}$ and $10\ \mu\text{m}$ light is distributed similarly on scales from 10 pc to 200 pc in M32.

ii) NGC 838

NGC 838 has a smooth envelope, but on good plate material it begins to show distorted outer isophotes and evidence for a disk. It is the fifth brightest galaxy in a group of 10, with NGC 839 as a companion. Disney and Wall (1977) have detected a 45 mJy radio source at 5 GHz in the nucleus. The source has a steep spectrum, and our VLA data shows it to be diffuse and extended with no strong compact component. The *IRAS* PSC fluxes quoted for NGC 838 are 0.60 Jy at $12\ \mu\text{m}$, 1.84 Jy at $25\ \mu\text{m}$, and a moderate quality flux of 17.39 Jy at $100\ \mu\text{m}$. The upper limit at $60\ \mu\text{m}$ is 0.36 Jy. The 12– $100\ \mu\text{m}$ energy distribution of NGC 838 appears from the *IRAS* data

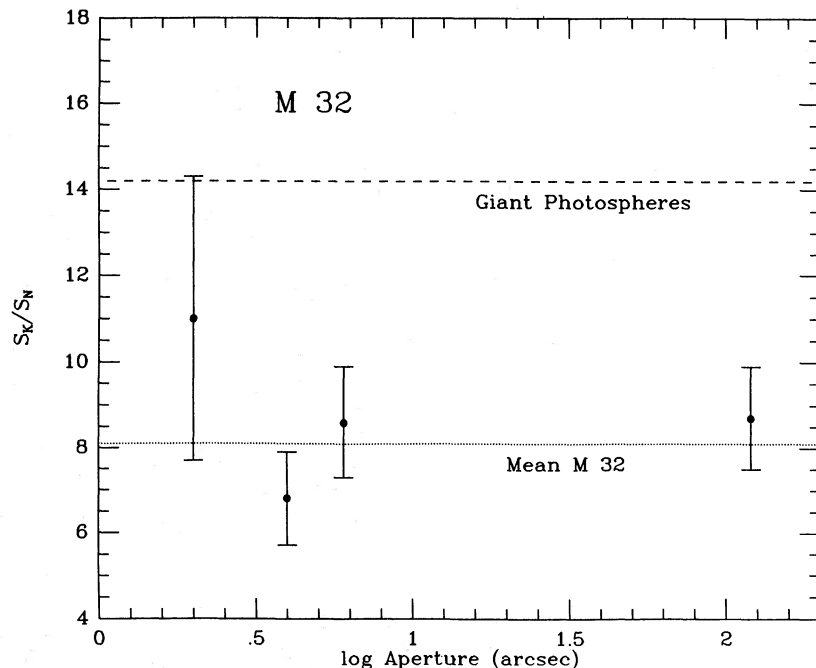


FIG. 2.—Ratio of $2.2 \mu\text{m}$ flux to $10 \mu\text{m}$ flux for M32 as a function of aperture size. The dotted line is the weighted mean flux ratio, and the dashed line is the ratio for M giant photospheric emission.

to be so remarkable that we are inclined to view the $60 \mu\text{m}$ flux density with some suspicion pending confirmation. Nevertheless, NGC 838 has a powerful source of far infrared emission.

iii) NGC 1052

The active elliptical NGC 1052 has a variable and compact radio component, strong nuclear emission lines, and a strong infrared excess (Wrobel 1985; Disney and Wall 1977). The excitation of the emitting line region has been successfully explained in terms of photoionization (Rose and Tripicco 1984). It is uncertain whether the infrared excess is due to reprocessed dust emission (Becklin, Tokunaga, and Wynn-Williams 1982) or the presence of a miniblazar in the nucleus (Rieke, Lebofsky, and Kemp 1982). The lack of $10 \mu\text{m}$ flux variability over a 15 yr period suggests that the far-infrared emission is due to dust grains; the measurement reported here agrees to better than 6% with the two previous data points. Unfortunately, the *IRAS* pointed observations on NGC 1052 have not fully resolved this issue (Neugebauer *et al.* 1984). The *Point Source Catalog* fluxes are listed in Table 1.

c) 1–4 Micron Colors

In order to study the spectral shape of the $10 \mu\text{m}$ excess, 47 galaxies from the $10 \mu\text{m}$ sample were measured at near-infrared wavelengths. Observations at *J*, *H*, *K*, and *L* sample the peak of the energy distribution of late-type stars. These new small-aperture measurements can be compared with the extensive set of multiaperture data on ellipticals published by Frogel *et al.* (1978) and Persson, Frogel, and Aaronson (1979). To do this we use a transformation between the two filter systems. The new near-infrared data are an important addition to previous work because these data are the first large set of measurements out to $3.8 \mu\text{m}$, and because the small aperture isolates the central few kiloparsecs of the galaxies. In terms of the average value of the projected aperture size, this work probes regions 4 times smaller than previous studies. Both of these

factors lead to a high sensitivity to weak nonthermal activity in the nucleus.

Two-color plots for the 47 ellipticals are shown in Figures 3

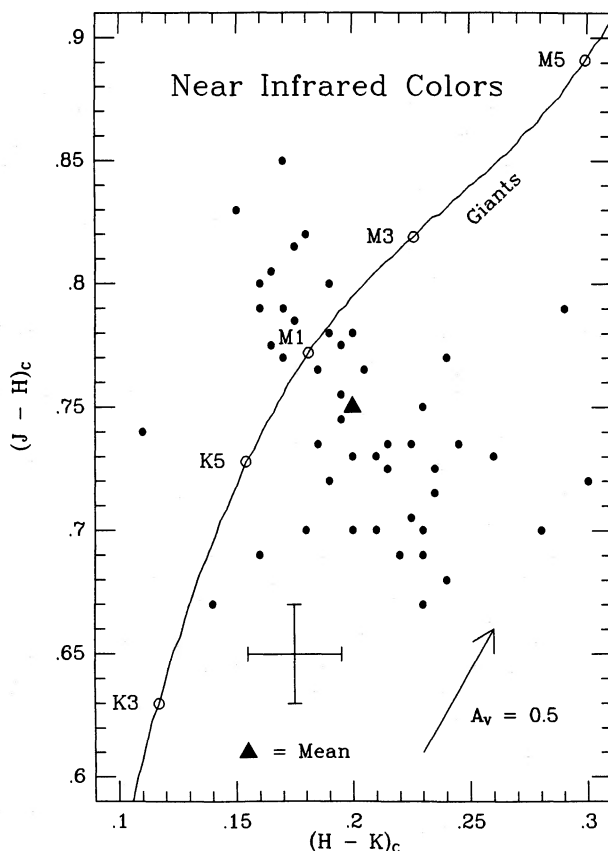


FIG. 3.—Two-color plot for elliptical galaxies: $J-H$ vs. $H-K$. The reddening vector and the locus of giant dwarf colors are shown.

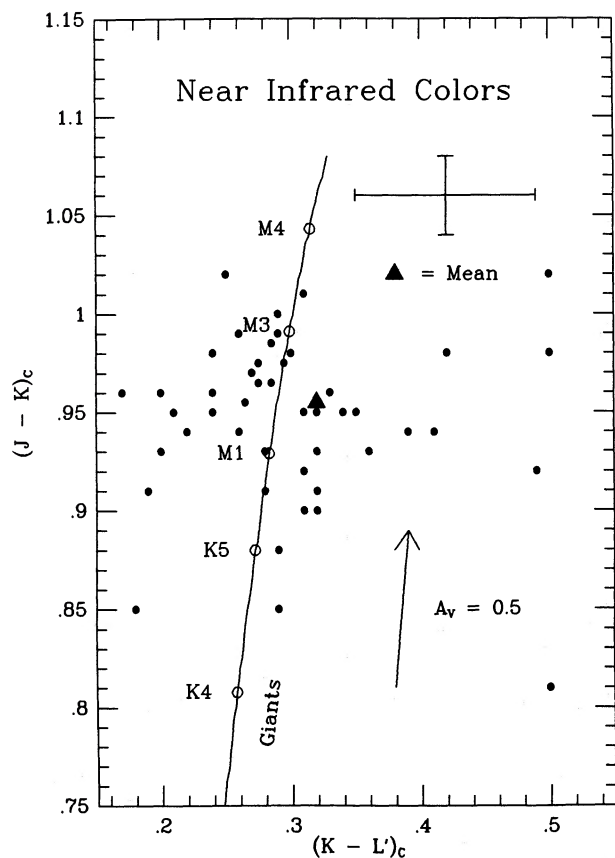


FIG. 4.—Two-color plot for elliptical galaxies: $J-K$ vs. $K-L$. The reddening vector and the locus of giant colors are shown.

($J-H$ vs. $H-K$) and 4 ($J-K$ vs. $K-L$). Superposed are the tracks for giants, with colors taken from the Appendix of Frogel *et al.* (1978). The ellipticals follow the track of expected giant color very closely, with mean colors corresponding to an M1 giant and a temperature of $T_{\text{eff}} = 3500\text{--}3700$ K. The mean colors are $J-H = 0.75 \pm 0.05$, $H-K = 0.20 \pm 0.04$, and $K-L = 0.32 \pm 0.11$ ($K-L = 0.22 \pm 0.08$). These $1\text{--}4 \mu\text{m}$ colors confirm the color gradient found by Frogel *et al.* (1978) and extend the measurement into smaller regions of the nucleus. The projected colors from the earlier work at our mean value of $\log A/D(0) = -1.45$ agree to within a few percent; $J-H = 0.73$ and $H-K = 0.22$ [note that the First Reference Catalog values of $\log A/D(0)$ in Frogel *et al.* 1978 must be adjusted by -0.3 to bring them into line with the RC2 values used in this paper]. The mean value of $J-K$ is 0.95 ± 0.05 at $\log A/D(0) = -1.45$, compared with $J-K$ of 0.88 ± 0.06 at a mean $\log A/D(0) = -0.25$ for the 15 largest aperture measures from the work by Frogel. Therefore there is a reddening by $\sim 7\%$ over a factor of 15 scale size in these galaxies. The red colors toward the center of ellipticals are usually interpreted as a metallicity gradient (Tinsley 1978). From the metallicity calibration in Frogel, Persson, and Cohen (1980), $J-K$ colors of 0.95 correspond to twice solar abundance for an IMF with $x \approx 1$.

The narrow dispersion of colors in Figures 3 and 4 is surprising. Only one or two giant subclasses are needed to account for the spread in all the colors; in fact the spread is not substantially larger than the observational errors. All but five galaxies lie within 3σ of the mean colors on both diagrams.

Internal reddening is unlikely to alter the colors significantly, because the color plot shows no larger scatter in the direction of the reddening vector than perpendicular to it. In both Figures 3 and 4, the rms dispersion of the data perpendicular to the reddening vector gives a limit to the mean internal reddening of $0.25\text{--}0.30$ visual mag. There is a remarkable degree of homogeneity in the stellar composition of elliptical galaxies.

d) Infrared Properties

The first possibility to consider is that the $10 \mu\text{m}$ emission is caused by the same process that produces the near-infrared radiation. The $10 \mu\text{m}$ photospheric emission from a K or M giant population can be predicted for each galaxy by extrapolation from the L point. Unfortunately, it is not obvious how to extrapolate reliably. It is well known that the near-infrared colors of ellipticals deviate strongly from the colors of a simple blackbody. Molecular effects such as H^- opacities affect the energy distributions of stars with $T_{\text{eff}} \leq 5000$ K, and Kurucz (1979) does not claim any great accuracy for his models in the infrared. Even for stars as hot as $T_{\text{eff}} = 18,000$ K, there is a large difference between the effective temperature and the color temperature fitted to the models ($T_c - T_{\text{eff}} = 3000$ K; Koornneef 1983). For cool giants, the deviations from blackbody behavior can be $25\%\text{--}35\%$ on a $J-H$ versus $H-K$ plot. A range of blackbody temperatures ($3300\text{--}4900$ K) is needed to fit the near-infrared data, and the fit is poor. A better procedure is to use standard giant colors to fit the galaxy data and provide an extrapolation to $10 \mu\text{m}$. The best empirical match to the ellipticals is the set of four late giants in the CIT standards list: β And (M0), $K-N = 0.20$; α Tau (K5), $K-N = 0.19$; μ UMa (M0), $K-N = 0.18$, and α Boo (K2), $K-N = 0.16$. They give a mean decrement of $S_K/S_N = 14.2$, which we shall adopt for extrapolating photospheres to $10 \mu\text{m}$. These four standards or Koornneef's giants give a fit to the ($J-H$) and ($H-K$) colors of the ellipticals with 10 times smaller residuals than blackbodies. The adopted decrement is redder than the Rayleigh-Jeans value of 21.5, and redder than other estimates of $S_K/S_N = 19.5$ by Rieke, Lebofsky, and Kemp (1982) and $S_K/S_N = 22$ by Rieke and Lebofsky (1978) and Puschell (1981a).

Using this decrement, the photospheric fluxes for 47 galaxies with $1\text{--}4 \mu\text{m}$ data can be predicted. The mean is $S_N = 3.1$ mJy. The only galaxy nearby and luminous enough to have a large predicted photospheric flux is M32 (NGC 221), with $S_N = 34$ mJy. Since the measured flux density is 62 mJy, the giant population is clearly detected in this galaxy. For the remaining galaxies, the contribution of photospheric emission to the observed $10 \mu\text{m}$ flux distribution can be determined. If the only contributor was photospheric emission, the expected flux distribution could be found by convolving the distribution of photospheric fluxes with the noise function. The observed distribution can be compared with the convolved distribution using the statistical tests employed in the last section. The Mann-Whitney U test indicates that the two distributions are different at the 99.6% level. There must be an additional contribution to the $10 \mu\text{m}$ fluxes; photospheres are not sufficient.

The flux at $2 \mu\text{m}$ lies near the peak of the giant energy distribution, so a correlation between the $2 \mu\text{m}$ and $10 \mu\text{m}$ radiation would be a strong indication that the long-wavelength excess is connected with the late-type stellar population. Figure 5 shows the ratio of 2 to $10 \mu\text{m}$ flux, and the two quantities are correlated at the 95% confidence level in a least

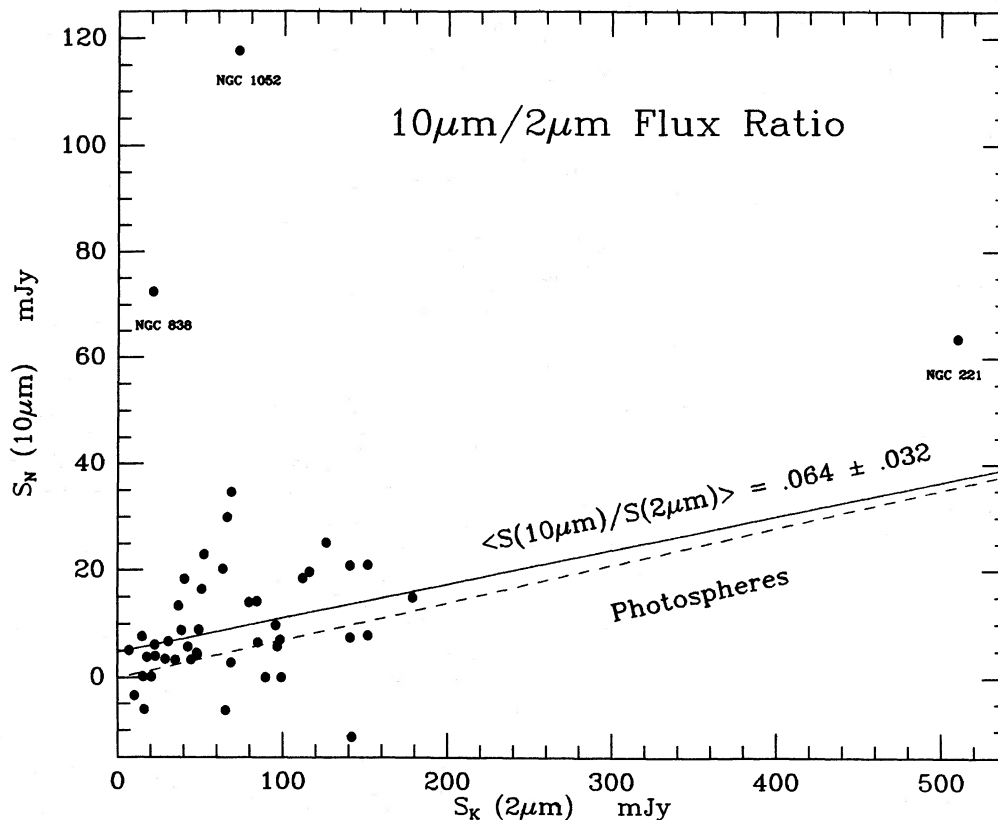


FIG. 5.—Flux at $10\ \mu\text{m}$ vs. $2\ \mu\text{m}$ flux for all 65 ellipticals in the sample. The line shows the mean value of $S(10\ \mu\text{m})/S(2\ \mu\text{m})$ for photospheres of giant stars.

squares linear regression. The galaxies NGC 838 and NGC 1052 are excluded because of their large contributions of nonphotospheric radiation at $10\ \mu\text{m}$, and NGC 221 is excluded because its proximity biases the correlation. A least-squares fit constrained to go through the origin gives $S_K/S_N = 8.9_{-1.2}^{+1.6}$, similar to the mean value for M32 in Figure 2. The photospheric decrement $S_K/S_N = 14.2$ is shown as a dotted line. The presence of an excess is confirmed by looking at Figure 5. If nothing more than photospheric emission was present, only NGC 221 would have an expected flux density of $S_N \geq 15$ mJy, instead of the 15 galaxies seen at that level.

e) Shape of the Infrared Spectrum: 1–10 Microns

The data can be combined to study the whole infrared energy distribution of the 47 galaxies measured from 1 to $10\ \mu\text{m}$. To demonstrate the level of the excess above giant photospheres in some of the galaxies, seven energy distributions are plotted in Figure 6. The expected energy distribution of the photospheric emission from late-type giants is also shown (as calculated in the last section). The 17 galaxies with complete data from 1– $10\ \mu\text{m}$ and $10\ \mu\text{m}$ significance of greater than $2\ \sigma$ can be used to crudely define the spectral shape of the excess flux. The procedure is to adopt giant colors which give a good fit to the 1– $3\ \mu\text{m}$ colors. The mean elliptical color of $J-K = 0.95$ corresponds to a flux ratio $S_J/S_K = 0.98$, and giants that fit this ratio predict $S_K/S_L = 2.13$ (Koorneef 1983). Therefore the adopted template flux ratio is $S_J/S_L = 2.09$, and the excess is defined as $\Delta S_L = S_L - S_J/2.09$. At $10\ \mu\text{m}$, the template flux ratio is $S_N/S_K = 14.2$, and the excess is defined as $\Delta S_N = S_N - S_K/14.2$. If the excess is less than 3 times the error in S_L (i.e., typically 9%–12%), an upper limit on the excess is

adopted. This is conservative since any displacement by $\sim 10\%$ in the S_K/S_L ratio would be readily noticed in Figure 4.

The ratio $\Delta S_L/\Delta S_N$ can be converted into two measures of the spectral shape of the excess: a power-law spectral index and an equivalent blackbody temperature. Table 3 contains the values of the excesses at L and N along with some derived quantities. Column (1) has the galaxy NGC number, and columns (2), (3) and (4) have the decrement S_K/S_N and the quantities ΔS_L and ΔS_N . Column (5) has the $10\ \mu\text{m}$ luminosity, calculated assuming $H_0 = 75\ \text{kms}^{-1}\ \text{Mpc}^{-1}$. In convenient units, $L_\nu(W) = 1.7 \times 10^{30} d^2$ (Mpc^2) S_ν (mJy), taking the bandwidth of the $10\ \mu\text{m}$ filter as 1.5×10^{13} Hz. Columns (6), (7), and (8) have the blackbody temperature and power-law spectral index of the nonphotospheric component, and the spectral index from $10\ \mu\text{m}$ to the GHz radio measurement. Since the aperture for the $10\ \mu\text{m}$ measurements and the VLA beam size are similar, the infrared-to-radio spectral index connects similar sized regions of the nucleus. Spectral indices are calculated assuming $S_\nu \propto \nu^{-\alpha}$. The resulting range of spectral indices in the infrared is $0.6 \leq \alpha \leq 2.2$, with the upper limits lying mostly in the range $\alpha \geq 1.5$. The corresponding range of equivalent blackbody temperatures is $500\ \text{K} \leq T \leq 700\ \text{K}$, and the upper limits are bounded by $T \leq 650\ \text{K}$. The $10\ \mu\text{m}$ errors propagate through to typical errors of $\Delta\alpha = \pm 0.5$ and $\Delta T = \pm 80\ \text{K}$. These numbers are biased toward steeper power laws and cooler blackbody temperatures by the low level of the $10\ \mu\text{m}$ detections. The immediate conclusion is that the equivalent temperature of the excess is far too low for it to be produced by photospheric emission from stars of any temperature. The minimum effective temperature of any hydrogen-burning main-sequence star is about 2700 K. There is a less

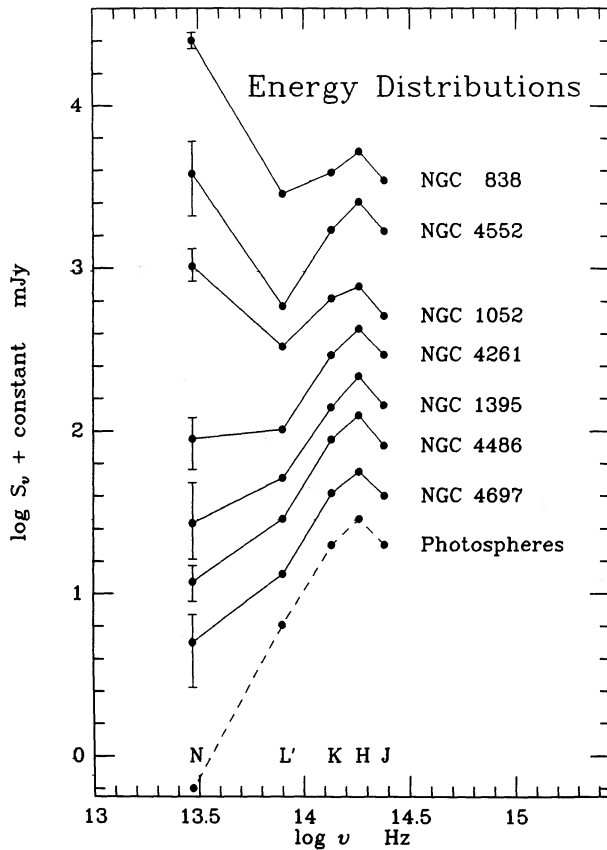


FIG. 6.—Energy distributions for some of the strongest 10 μm galaxies. The expected energy distribution from late giant photospheric emission is shown as a dotted curve.

convincing lower limit of > 250 K on the effective temperature of the excess, from the requirement that the 3–10 μm region not sit on a prohibitively steep part of the Wein tail of the blackbody curve.

f) Shape of the Infrared Spectrum: IRAS Data

Eleven of the 65 galaxies with ground-based 10 μm data have detections in one or more bands of the *IRAS Point Source Catalog*. Only two have detections in Band 1 (12 μm), but 10 have detections in either Band 3 or 4 (60 μm and 100 μm). The *IRAS* data complement the data obtained from the ground by being sensitive to very cool infrared components. Table 4 summarizes the *IRAS* data. We note that the 25 μm flux for M32 has recently been redetermined using high-quality pointed observations, with the result that the flux of 0.07 Jy quoted by Habing *et al.* (1984) has been adjusted to 0.18 Jy (R. Walterbos 1986, private communication). With that exception, all other fluxes in Table 4 are taken from the *Point Source Catalog*. Columns (1)–(5) show the galaxy name, the 12 μm flux $S_{12\mu\text{m}}$ and the flux ratios $S_{25\mu\text{m}}/S_{12\mu\text{m}}$, $S_{60\mu\text{m}}/S_{12\mu\text{m}}$, and $S_{100\mu\text{m}}/S_{12\mu\text{m}}$. No color correction has been applied because it is generally less than 5%. For the mean energy distributions of ellipticals, $S_K/S_{12\mu\text{m}} \approx 0.8 (S_K/S_N)$. The decrement $S_K/S_{12\mu\text{m}}$ is in column (6) and can be compared with column (2) in Table 3. To determine this flux ratio, 2.2 μm fluxes are taken from Frogel *et al.* (1978) and extrapolated to an equivalent of 120" using their curve of growth. The extrapolation is normally less than 0.3 in $\log A/D(0)$, although in two cases the 2.2 μm flux presented in this paper is extrapolated by 1.3 in $\log A/D(0)$. Therefore the decrement $S_K/S_{12\mu\text{m}}$ in Table 4 holds over kpc scales in the galaxy compared with the 100 pc scales referred to in Table 3. Column (7) gives the bounds in microns between which the spectral index in column (8) is calculated. The *IRAS* spectral index in column (8) can be compared with the shorter wavelength 4–10 μm spectral index in column (7) of Table 3.

g) Extended 10 Micron Emission in M32

As the closest galaxy in the sample, M32 offers potentially the most important clue to the emission process in ellipticals at 10 μm . It is the only galaxy where the radial distribution of the 2–10 μm flux density can be studied. Two important conclusions can be drawn from Figure 2. First, the ratio of 2 μm to 10 μm flux is constant with radius. Therefore, the agent

TABLE 3
INFRARED SPECTRUM: 1–10 MICRONS

Galaxy (1)	S_K/S_N^a (2)	$\Delta S_{L'}$ (mJy) (3)	ΔS_N (mJy) (4)	10 μm Luminosity ^b (W) (5)	$T_{4-10\mu\text{m}}$ (K) (6)	$\alpha_{4-10\mu\text{m}}$ (7)	α_r^{rad} (8)
NGC 221	8.6	<13.2	31.2	9.7×10^{30}	<550	>1.5	< -0.42
NGC 584	5.7	<2.3	8.4	1.5×10^{34}	<530	>1.6	< -0.27
NGC 596	3.1	<3.2	12.9	2.2×10^{34}	<550	>1.4	< -0.28
NGC 838	0.3	8.4	71.0	3.3×10^{35}	470	2.2	-0.05
NGC 1052	0.7	20.4	112.0	7.3×10^{34}	510	1.8	+0.16
NGC 1395	3.1	<2.8	15.7	1.5×10^{34}	<510	>1.8	-0.23
NGC 1587	2.7	<1.9	10.8	5.9×10^{34}	<510	>1.8	+0.19
NGC 2693	2.2	<2.2	15.6	1.4×10^{35}	<480	>2.0	-0.22
NGC 3379	11.9	<5.5	2.4	2.6×10^{33}	-0.20
NGC 4261	2.2	<4.2	25.2	4.0×10^{34}	<510	>1.8	+0.20
NGC 4278	6.0	<5.3	10.6	2.4×10^{33}	<670	>0.7	+0.33
NGC 4374	6.7	6.4	11.0	4.6×10^{33}	700	0.6	+0.52
NGC 4473	5.9	<3.4	11.5	2.9×10^{34}	<570	>1.3	< -0.30
NGC 4486	2.0	7.4	29.8	1.5×10^{34}	550	1.4	+0.34
NGC 4552	7.2	4.6	10.4	1.7×10^{32}	650	0.8	+0.11
NGC 4697	5.0	<7.6	16.4	1.0×10^{34}	<650	>0.8	< -0.33
NGC 5557	2.3	<4.2	19.2	7.5×10^{34}	<540	>1.5	< -0.32

^a S_K/S_N corrected to aperture size of 6".

^b Luminosities calculated assuming $H_0 = 75 \text{ km s}^{-1} \text{ Mpc}^{-1}$.

TABLE 4
INFRARED SPECTRUM: IRAS DATA

Galaxy (1)	$S_{12\ \mu\text{m}}$ (mJy) (2)	$S_{25\ \mu\text{m}}/S_{12\ \mu\text{m}}$ (3)	$S_{60\ \mu\text{m}}/S_{12\ \mu\text{m}}$ (4)	$S_{100\ \mu\text{m}}/S_{12\ \mu\text{m}}$ (5)	$S_K/S_{12\ \mu\text{m}}^a$ (6)	Band A/B and B (μm)/(μm) (7)	α_{IRAS} (8)
NGC 221	390	0.5	0.9	4.1	19.9	12/25	< -0.4
NGC 205	<250	>11.1	>1.2	25/100	>1.7
NGC 838	600	3.07	<0.6 ^b	29.0	0.2	12/25	1.5
NGC 1052	<300	>1.8	>3.1	>4.6	>2.0	25/60	0.6
NGC 4125	<340	...	>1.8	>3.9	...	60/100	1.5
NGC 4278	<250	...	>2.2	>6.2	>2.8	60/100	1.9
NGC 4374	<430	...	>1.2	...	>2.7	12/60	>0.1
NGC 4406	<250	>1.4	3.2	2.3	>4.0	25/100	1.4
NGC 4476	<250	...	>2.3	>6.2	>0.5	60/100	1.9
NGC 4486	<480	...	>1.0	...	>6.1	25/60	>0.3
NGC 5118	<250	...	>4.0	>7.3	>2.1	60/100	1.2

^a $S_K/S_{12\ \mu\text{m}}$ corrected to aperture size of $120''$.

^b Suspicious $60\ \mu\text{m}$ flux; see § IVf.

responsible for the $10\ \mu\text{m}$ radiation is distributed similarly in the galaxy to the giant stars that dominate the radiation at $2\ \mu\text{m}$. Second, the flux ratios S_K/S_N in all apertures are lower than the canonical value for photospheres of late type giants, $S_K/S_N = 14.2$. The weighted mean of the 3 IRTF and 1 IRAS measures is $S_K/S_N = 8.1$, indicating 80% more $10\ \mu\text{m}$ flux than would be expected from giant photospheres. Table 3 indicates that nonphotospheric $10\ \mu\text{m}$ emission is present in most of the stronger $10\ \mu\text{m}$ detections. In other words, Figure 2 indicates not only an excess above photospheres at $10\ \mu\text{m}$ in M32, but it indicates that the excess is extended. Caution is advisable in generalizing the results for M32 to larger and more luminous galaxies, but M32 is clearly a crucial test case. If this holds for the other ellipticals, then it is unlikely that the $10\ \mu\text{m}$ radiation

is connected with an unresolved compact radio source in the galaxy center. By inference, the $10\ \mu\text{m}$ excess in other ellipticals may derive from the giant population that dominates at $2\ \mu\text{m}$.

h) Correlation with Radio and Optical Data

With new VLA data, all of the NGC galaxies have radio measurements of their nuclei sensitive to compact emission of 1 mJy ($5\ \sigma$) or more at 5 GHz. Forty-one out of the 65 galaxies are detected with $S_{\text{rad}} \geq 1\ \text{mJy}$. The detection rate compares favorably with the 22 out of 65 having $S_N/\sigma(S_N) \geq 2$, so it is of interest to see whether the infrared and radio emission is correlated. In Figure 7, radio flux is plotted against $10\ \mu\text{m}$ flux with the adopted detection limits marked. The average relationship between $10\ \mu\text{m}$ flux and radio free-free flux in spiral galaxies

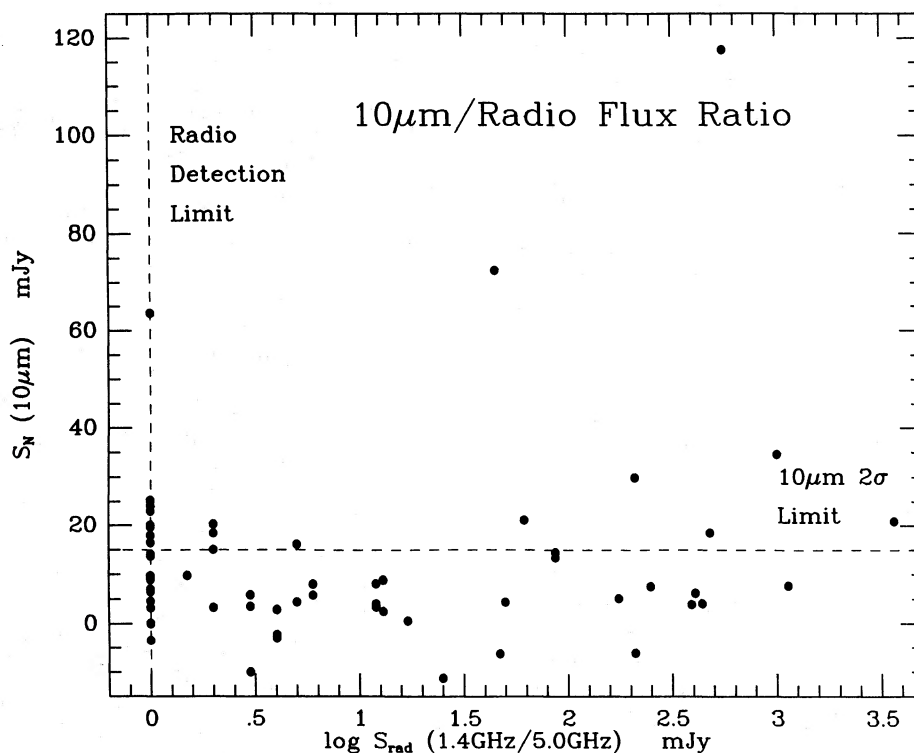


FIG. 7.—Flux at $10\ \mu\text{m}$ vs. GHz radio flux for all 65 ellipticals in the sample. The infrared and radio detection limits are shown.

with active star formation would be a nearly vertical line in Figure 7. From measures of the central regions of five spiral galaxies in Wynn-Williams and Becklin (1985), the ratio $S_N/S_{\text{ff}} \approx 40$. Only NGC 221 has a larger ratio, and most ellipticals have $10 \mu\text{m}/\text{radio}$ flux ratios much too low to be produced by typical star formation processes in spirals. Only 12 ellipticals are detected at *both* radio and infrared wavelengths, consistent with a random subset of each set of detections. We test for a relationship between radio and infrared emission by performing a nonparametric ranking test on all the data, including upper limits. There is no tendency for sources with $S_N/\sigma(S_N) > 2$ to have stronger radio emission than sources with $S_N/\sigma(S_N) < 2$, nor is there any significant difference between the $10 \mu\text{m}$ fluxes of sources with $S_{\text{rad}} > 50 \text{ mJy}$ and $S_{\text{rad}} < 50 \text{ mJy}$ ($< 60\%$ confidence level).

All of the galaxies in the sample have measured redshifts and many have optical photometry or morphological information, so the infrared and optical properties can be compared. Using information compiled from RC2, Tonry and Davis (1981), Davies *et al.* (1983), Davies and Illingworth (1983), Schechter and Gunn (1979) and references therein, the presence of detectable $10 \mu\text{m}$ emission was compared with many global optical parameters such as ellipticity, optical size, mass-to-light ratio, or total optical luminosity. Linear regression reveals no correlation in each case. The presence of $10 \mu\text{m}$ emission does not appear to be correlated with morphological peculiarity in the parent galaxy. We have also divided the sample according to environment, into galaxies in clusters, in groups, and in the field. The three sets have roughly equal numbers and mean distances. There is no tendency for strong $10 \mu\text{m}$ emission to be preferentially associated with a specific environment (despite individual cases such as NGC 838 where the infrared power is probably an indirect result of interaction with another galaxy). In general, the conditions necessary to create strong $10 \mu\text{m}$ emission are generated *within* the galaxy.

Rose (1986) has presented strong limits on the number of young stars and the recent star formation history of 11 elliptical galaxies, 10 of which are included in this paper. Three of the galaxies in common to the two studies (NGC 221, 584 and 5557) are among the stronger $10 \mu\text{m}$ sources. Therefore, in those cases at least, the $10 \mu\text{m}$ radiation is unlikely to be generated by dust and gas associated with a recent generation of star formation. Rose has also searched for very weak nuclear activity through the [O III] $\lambda 3727$ line in a larger sample of galaxies, 25 of which are in common with this study. Ten have had [O III] $\lambda 3727$ detected in their nuclei. The same number are $10 \mu\text{m}$ detections. Six galaxies have both $10 \mu\text{m}$ emission and [O III] emission, so there is no strong connection between the two properties. Moreover, the three galaxies with high [N II]/H α ratios in the sample (indicative of high nuclear excitation, possibly by a photoionizing power law) are all nondetections at $10 \mu\text{m}$.

V. DISCUSSION

a) Nonthermal Radiation

One exciting possibility is that the unexpected level of $10 \mu\text{m}$ radiation in many elliptical galaxies is caused by modest versions of the extreme nuclear activity seen in distant quasars and radio galaxies. Recently, observational interest in the weak end of the luminosity function of active galactic nuclei has exploded. The NGC galaxies have $10 \mu\text{m}$ luminosities of order $10^{39} \text{ ergs s}^{-1}$ (i.e., $\sim 10^{32} \text{ W}$). At the other end of the spectrum of power the blazars (luminous, variable radio sources with

strong nonthermal infrared continua) have $10 \mu\text{m}$ luminosities up to 10^{46} – $10^{47} \text{ ergs s}^{-1}$ (Impey *et al.* 1984). A moderate proportion of nearby ellipticals show evidence for the infrared excess, while the space density even of modest luminosity blazars is less than 10^{-6} Mpc^{-3} (Schwartz and Ku 1983), and the space density of the extreme blazars is much lower. The two sets of objects cover a range of 8 decades of luminosity and more than 5 decades of space density. Is it possible that we are observing mini-active galactic nuclei?

If there are any mini-AGN in these ellipticals, they are completely dominated by stellar radiation in the near-infrared. However, since the power laws typical of AGN rise and the stellar photospheric flux falls with increasing wavelength, the visibility of a weak nonthermal component will improve toward $10 \mu\text{m}$. We begin by making a comparison between the spectral shape of the $10 \mu\text{m}$ excess radiation in the ellipticals and the spectral shapes of well-studied types of AGN. From data compiled in the literature, the mean 1– $10 \mu\text{m}$ spectral indices of AGN are Seyfert 2: $\alpha = 2.30 \pm 0.62$ (nine objects, Rieke 1978); Seyfert 1: $\alpha = 1.49 \pm 1.01$ (26 objects, Rieke 1978); quasars: $\alpha = 1.25 \pm 0.28$ (22 objects, Neugebauer *et al.* 1979), and blazars: $\alpha = 1.11 \pm 0.28$ (29 objects, Neugebauer *et al.* 1979; Cruz-Gonzales and Huchra 1984). Over 75% of the galaxies in Table 3 have $\alpha_{\text{IR}} \geq 1.40$, and 35% must be steeper than 1.80. Spectral indices covering different wavelength ranges in the infrared are comparable because most AGN have little spectral curvature in the infrared. Over the longer wavelength baseline of the IRAS data, over 50% of the galaxies in Table 4 have $\alpha_{\text{IR}} \geq 1.40$. Therefore the infrared spectra in the ellipticals are significantly steeper than those of quasars or blazars.

Heckman *et al.* (1983) have found a strong correlation between the 6 cm nuclear flux and the nonstellar $2.2 \mu\text{m}$ flux in a set of nearby radio galaxies with compact radio sources. There is also a tight relation between the 6 cm and $10 \mu\text{m}$ fluxes of BL Lac objects or blazars, sources where the variability and polarization of the continuum makes it certain that both the radio and infrared emission is synchrotron radiation. The lack of a correlation between radio and $10 \mu\text{m}$ fluxes (Fig. 7) does not directly rule out nonthermal emission in the infrared. When integrated 6 cm fluxes are plotted against (nonsimultaneous) $10 \mu\text{m}$ fluxes for a set of 19 BL Lac objects, there is also no correlation (Cruz-Gonzales and Huchra 1984; C. D. Impey, G. Neugebauer, and G. A. Miley, in preparation). Since good core fluxes at a high radio frequency are not available for the weaker ellipticals, the comparison must be made between $10 \mu\text{m}$ emission and total radio flux measured at a relatively low frequency. The scatter in the infrared/radio plot will then be substantial, because 6 cm is far removed from the frequency at which the most compact synchrotron component becomes optically thin.

Another test is to compare the distribution of spectral indices between the radio (6 cm) and the infrared ($10 \mu\text{m}$). The mean value for BL Lac objects or blazars is $\alpha_{\text{ir}}^{\text{rad}} = 0.35 \pm 0.11$, compared to $\alpha_{\text{ir}}^{\text{rad}} = 0.11 \pm 0.28$ for the ellipticals. Many of the ellipticals detected at both wavelengths have inverted spectra, i.e., the infrared flux density exceeding the radio flux density. The lower detection limit at 6 cm than at $10 \mu\text{m}$ of course leads to a bias toward lower values of $\alpha_{\text{ir}}^{\text{rad}}$. However, even if the weak radio sources with higher $\alpha_{\text{ir}}^{\text{rad}}$ could be detected, the *distributions* of $\alpha_{\text{ir}}^{\text{rad}}$ for blazars and ellipticals must be different. This weak evidence against mini-blazars in elliptical galaxies cannot be extended to rule out

weak analogs of the optically selected quasars (which far outnumber the radio-loud quasars and blazars). The majority of quasars do not vary, are not polarized and do not have completely smooth power-law spectra. The emission mechanism is still unknown, though it is presumed to be synchrotron emission. Since the radio/optical luminosity ratio of quasars can vary by over a factor of a thousand (Condon *et al.* 1981), intrinsic scatter will wipe out any correlation in Figure 7. The spectral energy distributions of optically selected quasars from Condon *et al.* (1981) and Neugebauer *et al.* (1979) give a mean spectral index of $\alpha_{\text{ir}}^{\text{rad}} = 0.15 \pm 0.32$, indistinguishable from the value for the ellipticals.

The evidence from energy distributions alone argues only weakly against nonthermal infrared activity in the cores of the elliptical galaxies. Measures of polarization or variability would point strongly to the synchrotron process. Unfortunately, the sources are too weak at $10 \mu\text{m}$ and the excess is too heavily diluted by starlight at shorter wavelengths to make the observations feasible. If the $10 \mu\text{m}$ elliptical sources turn out to be nonthermal mini-AGN, it will have a profound effect on current theories of nuclear activity. One popular view is that nuclear activity is episodic in galaxies and is triggered by favorable conditions such as a deep gravitational potential well in the nucleus, or a close encounter with another galaxy. The discovery of a smooth spectrum of nuclear activity right down to ubiquitous but anemic activity in most galaxies would imply that *all* galaxies have the capability for nuclear activity.

b) Hot Dust in Ellipticals

Elliptical galaxies are traditionally viewed as dynamically simple systems with one coeval stellar population and little evidence for young stars or large amounts of dust and gas. The two strongest $10 \mu\text{m}$ detections, NGC 838 and NGC 1052, both show signs of interaction and morphological peculiarity. For example, X-ray coronae at the centers of some ellipticals indicate a substantial mass of gas at 10^6 – 10^7 K. When high contrast images are available, many ellipticals reveal small dust lanes in their nuclei. Sadler and Gerhard (1984) have agreed that $\sim 40\%$ of all ellipticals have nuclear dust lanes with sizes of a few kiloparsecs and masses 10^4 – $10^6 M_{\odot}$. Jedrzejewski (1985) has found dust features in $\sim 30\%$ of a sample of 49 ellipticals, using ratios of CCD frames in the *B* and *R* filters. Despite the ubiquity of nuclear dust lanes in ellipticals, two examples show that detectable $10 \mu\text{m}$ emission does not always result from the presence of dust. NGC 3377 is a relatively normal galaxy with no detected radio source and no emission lines, and an upper limit to the $10 \mu\text{m}$ flux. Yet the CCD frame ratio clearly shows an asymmetric dust lane at the nucleus. NGC 5813 also has no detected $10 \mu\text{m}$ flux, but it has extensive dust features near the nucleus and may be a merger remnant.

The equilibrium condition for an optically thin dust cloud can be used to calculate a lower limit on the size of the cloud. The peak absorption wavelength is taken to be $0.3 \mu\text{m}$ and an efficiency law of $\epsilon \approx \lambda^{-1}$ is assumed. The observed upper limit on the temperature of the $10 \mu\text{m}$ excess is $T \leq 700$ K, corresponding to a dust cloud size of $R \geq 2 \times 10^{16}$ cm. The lower limit comes from the Wein limit in the infrared and the requirement that high levels of $60 \mu\text{m}$ flux are not observed by *IRAS*. This weaker constraint is $T \geq 300$ K leading to a size upper limit of $R \leq 1 \times 10^{17}$ cm. The corresponding light travel time and minimum variability time scale is about 10 days. A single dust cloud could produce the required flux in an unresolved

region at the center of the galaxy; the mass of grains necessary to maintain the pressure balance is only $10^{-5} M_{\odot}$ (where $\rho_{\text{gas}}/\rho_{\text{dust}} \approx 300$ for graphites and silicates). The most important distinction to make when modeling heated dust is whether or not the dust is *close* to the stars. The aperture for the $10 \mu\text{m}$ observations subtends a diameter of 1–2 kpc at the average distance of the NGC galaxies. From measurements of 19 ellipticals in our sample, the mean stellar density within 1 pc of the center is $\log \rho = 3.86 \pm 0.28 (L_{\odot} \text{pc}^{-3})$ (J. L. Tonry, private communication). The corresponding mean stellar separation is 2×10^{17} cm (0.07 pc). This is a lower limit since it is derived by fitting a cusp density profile to data that is unresolved near the nucleus. In reality, the density profiles of ellipticals probably flatten near the center, with a corresponding increase in the stellar separation (Schweizer 1979). Therefore, stars in the galaxy nucleus are too widely separated to heat intervening dust to the required temperature. Emission from heated dust will only be important if the dust is close to the stars, perhaps in the form of circumstellar shells.

A caveat to the previous argument concerns the possibility of the $10 \mu\text{m}$ radiation coming from small dust grains. Sellgren (1984) has described grains in the interstellar medium with very low heat capacity, which can be heated temporarily to ~ 300 K by the absorption of a single UV photon. Unlike large dust grains, these particles reach a temperature that is independent of the distance to the heating source. It can easily be shown that the ambient UV radiation field in the nuclei of ellipticals is far smaller than that in spirals, and that small grain heating is unlikely to occur. For example, NGC 4472 has a strong flux at 1500 \AA that indicates 3×10^3 OB stars with $M_B \approx -4$ (Bertola and Oke 1982); a space density of ionizing stars several orders of magnitude lower than in star forming spirals. Also, Coleman, Wu, and Weedman (1980) have published energy distributions for different galaxy types in the UV, and when normalized at 4500 \AA , the relative amounts of flux at 2000 \AA are: $S(\text{Sbc})/S(\text{E}) \approx 10$, $S(\text{Scd})/S(\text{E}) \approx 23$, $S(\text{Im})/S(\text{E}) \approx 45$. Using published energy distributions of ellipticals from 1200 \AA to $2 \mu\text{m}$, and the mean flux ratio of $S_N/S_K = 0.064$, we can calculate the power per unit bandwidth (νS_{ν}) at 1200 \AA and $10 \mu\text{m}$. In galaxies with the strongest UV turn-ups (NGC 4472, NGC 3379), the two powers are similar. However, the energy in hard UV flux in most ellipticals fails by an order of magnitude to match the $10 \mu\text{m}$ luminosity. Even assuming highly efficient conversion of UV to $10 \mu\text{m}$ energy, small dust grains seem inadequate to account for the detected $10 \mu\text{m}$ emission.

We can also rule out $10 \mu\text{m}$ radiation due to free-free emission in active star-forming regions. The stronger $10 \mu\text{m}$ sources should then show 6 cm emission of 1–3 mJy, above the detection limit of the VLA data. The lack of radio detections among the strong $10 \mu\text{m}$ sources argues against free-free emission. Following Scoville *et al.* (1983) we can calculate N_{Lyc} for the mean luminosity of the sample, $N_{\text{Lyc}} \approx 5 \times 10^{52} \text{ s}^{-1}$. The number of OB stars in a Salpeter Initial Mass Function needed to generate the appropriate $10 \mu\text{m}$ luminosity can be directly estimated (Ryter and Puget 1977). Using the relationship between far infrared and total luminosity of Scoville *et al.* (1983), the luminosity in young stars is $L_* \approx 8 \times 10^8 L_{\odot}$. The mean diameter subtended by our $6''$ aperture typically encloses 30% of the light of an elliptical. Dynamical studies in elliptical nuclei show a typical M/L of 15, in a galaxy with total luminosity $10^{10} L_{\odot}$. The $10 \mu\text{m}$ data therefore requires about 25% of the nuclear luminosity to be produced by massive young

stars. Anything close to that level of star formation can be ruled out with great confidence.

c) Dust Associated with Evolved Giants

The late stages of giant evolution are accompanied by mass-loss processes which are known to give rise to an infrared excess (e.g., Renzini 1977). The observation in M32 that the excess $10\ \mu\text{m}$ emission follows the stellar distribution makes it attractive to consider dust associated with mass loss from evolved giants as the cause of the $10\ \mu\text{m}$ emission in ellipticals. Reimers (1975) has shown that there is a $10\ \mu\text{m}$ excess (over photospheric emission) in essentially *all* stars cooler and more luminous than an envelope in the H-R diagram defined by M6 III, M5 II, M1 Iab, G8 Ia, G0 Ia⁺. An excess is observed in all long-period variables, and in many nonvariable late-type giants (Hagen 1978; Dyck, Lockwood, and Capps 1974). The physical details of the mass-loss process in giants are complex and only partially understood. However, since we are dealing with large stellar populations, we will take a morphological approach to the question of mass loss. Reimers (1974) has shown that mass loss depends in a simple way on basic stellar parameters. He defined a relationship $\dot{M}\ (M_{\odot}\ \text{yr}^{-1}) \approx 4 \times 10^{-13} L/gR$, where \dot{M} is the mass-loss rate, and L , g and R are the luminosity, gravity, and radius of the star in solar units. This empirical result holds over a factor of over 10^4 in mass-loss rate, and for mass losses determined by completely different methods. The physical interpretation of the relationship is that different stars use the same fraction of their luminosity ($\sim 10^{-5}$) to provide the potential energy necessary to eject material from the stellar surface to infinity. Reimers also noted a relationship $S_N/S_L \propto \dot{M}$, which offers the interesting possibility of using infrared excess to discriminate between stars in the same part of the H-R diagram. A $10\ \mu\text{m}$ excess is therefore expected from the basic mass-loss relation $\dot{M} \propto L/gR$ and a reasonable range of dust shell parameters. The observational limit where a $10\ \mu\text{m}$ excess begins to be seen corresponds to $L/gR \geq 1.5 \times 10^5 L_{\odot}/g_{\odot} R_{\odot}$ or $\dot{M} \geq 6 \times 10^{-8} M^{-1}$. To determine whether normal mass loss processes in giants can generate the $10\ \mu\text{m}$ radiation observed in the nuclei of ellipticals, we first summarize the observational evidence on the infrared excess in individual stars. Second, we combine the stellar types to form a model elliptical galaxy, using the bulge population of our own galaxy in Baade's Window as a template. Finally, the required stellar populations are viewed more broadly in terms of stellar evolution and global mass loss rate within a galaxy.

i) Infrared Colors of M Giants

Figure 8a is a flux ratio plot of late type giants compiled from many examples in the literature. Flux ratios are in terms of the L filter because the L filter was not being widely used when most of the measurements were made. The data from different telescope/filter combinations have been reduced to a homogeneous set of flux ratios using color transformations mostly from Koornneef (1984) and the flux calibrations described in this paper. The residual errors in the flux ratios due to this process are approximately 10%, a level which does not affect the arguments that follow. Variability information is admittedly incomplete. The mean flux ratios of normal giant photospheres are marked, as are the colors of blackbody components and power-law components. The flux ratio S_K/S_L is sensitive to hot thermal components ($T \geq 4000\ \text{K}$) and the flux ratio S_N/S_L is sensitive to cool thermal components

($T \leq 1000\ \text{K}$). The scatter of the data points for the giants shows that the circumstellar dust shell is almost always cooler than 600 K. Flux ratio diagrams allow the decomposition of multiple components. For example, if a chord is drawn from the mean photospheric color (i.e., M3) through the data point, then it will intersect the blackbody curve at the temperature of the excess component. The relative contributions of the photospheric and thermal components are given by the ratio of the distance from the data point to the photospheric and thermal flux ratios respectively. In Figure 8b, the same flux ratios are plotted for the ellipticals, and the envelope containing 90% of the giant observations is shown for comparison. As with the giants, the excess is very cool, because it shows mostly in the S_N/S_L ratio. The areas occupied by the giants and ellipticals are adjacent, but they do not overlap, since the ellipticals have a mean spectral type of M1 or M2 and the giants have a mean spectral type of M8. Most of the scatter of the elliptical data in Figure 8b is observational, so in the comparison with Baade's Window models we will only fit the mean flux ratios and not the range in the flux ratios.

To build a synthetic elliptical in the infrared, consider the infrared flux ratios as a function of spectral type. The reddest color for a given M subclass increases from $S_K/S_L = 1.5$, $S_N/S_L = 0.4$ for M2 types to $S_K/S_L = 0.5$, $S_N/S_L = 3.0$ for M8 types. Beyond subclass 8 there is a large scatter of colors. The optical/infrared colors for these giants have an even larger range as a function of spectral subclass. The mean color for a given M subclass increases from $S_V/S_K = 10^{-1}$, $S_V/S_N = 1$ for M2 types to $S_V/S_K = 10^{-5}$, $S_V/S_N = 10^{-6}$ for M8 types. Over the long baseline from $0.55\ \mu\text{m}$ to $10\ \mu\text{m}$, very late M giants contribute a million times more $10\ \mu\text{m}$ flux than the earliest M giants. Therefore, photometry or spectrophotometry anywhere in the optical region is insensitive in detecting the latest stellar types in a galaxy. Yet these stars may dominate the infrared output.

ii) Population Synthesis using Baade's Window

It is likely that the galactic bulge is a good model for the old population in elliptical galaxies. Blanco, Frogel, and collaborators have been pursuing a large program to unravel the properties of the Baade's Window (BW) giants (Blanco, Blanco, and McCarthy 1978; Blanco, McCarthy, and Blanco 1984; Frogel, Cohen, and Persson 1983). The SAAO group have also been selecting (Mira) variables in the same field (Lloyd-Evans 1976). Baade's Window is surprisingly deficient in carbon stars compared to other giant populations (the ratio of carbon stars to M giants $(C/M)_{\text{BW}} = 0.003$ vs. $(C/M)_{\text{LMC}} = 1.9$ and $(C/M)_{\text{SMC}} = 36$ in the Magellanic Clouds), so they will be neglected in this discussion. The grism search of Blanco, McCarthy, and Blanco (1984) is complete to $I \approx 14.8$ and sees right through the nuclear bulge (i.e., samples most of the luminosity function out to beyond 10 kpc). The search is complete only for types later than M6, since the grism technique requires high contrast in the TiO bands for detection of giants. 10%–15% of the grism giants are long period variables (LPV), and the proportion increases with spectral subclass from $\sim 15\%$ at M6 to essentially 100% at M9. Infrared photometry from Frogel, Whitford, and Rich (1984, and unpublished) shows that the late-type variables in BW are similar to solar neighborhood Mira variables with OH emission and circumstellar shells. Altogether, over 300 giants M6 or later have been cataloged by Blanco, McCarthy, and Blanco (1984).

The M giant luminosity function in Baade's Window can be

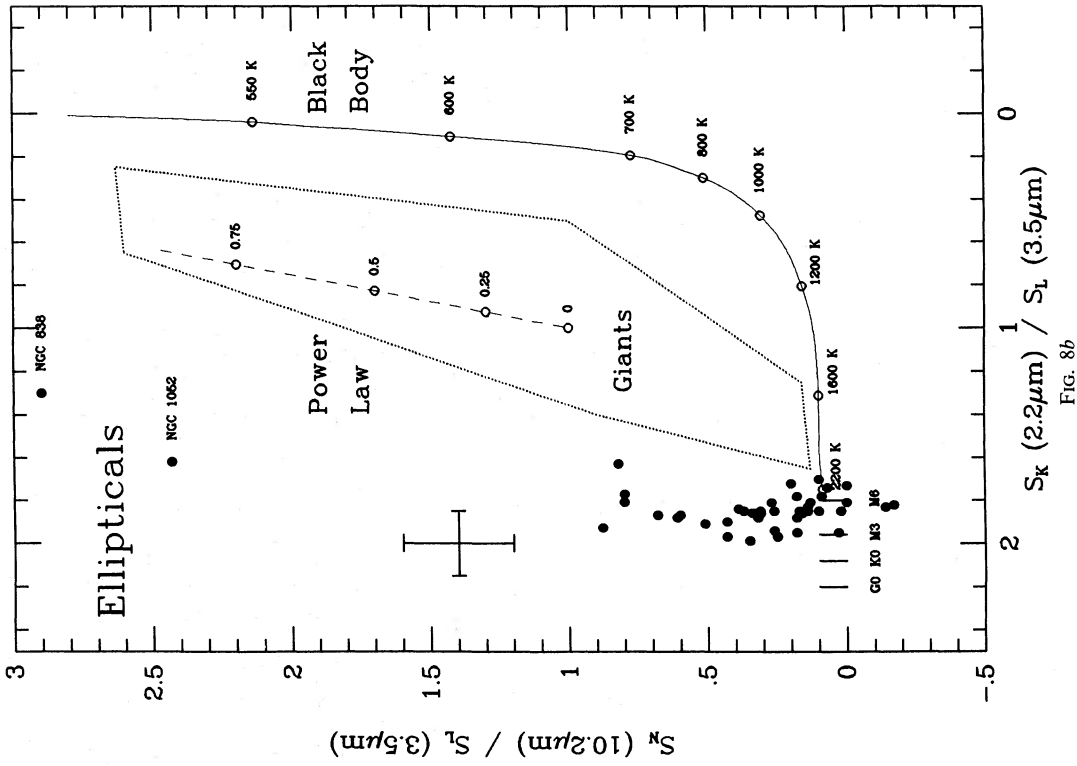


FIG. 8a

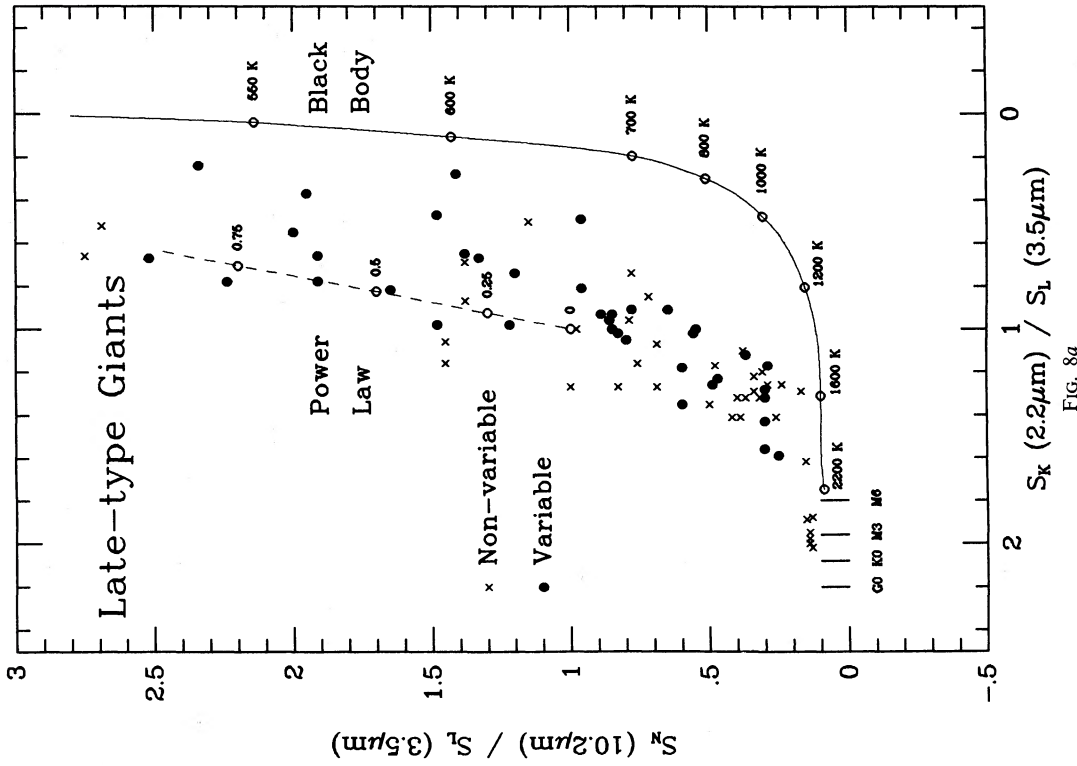


FIG. 8b

FIG. 8.—(a) Flux ratio plot for late-type giants: S_N/S_L vs. S_K/S_L . Variable and nonvariable sources have different symbols, and the locus of blackbody flux ratios is shown. (b) Flux ratio plot for elliptical galaxies: S_N/S_L vs. S_K/S_L . The envelope encompassing 90% of giant colors is shown, along with the loci of blackbody and power-law flux ratios.

constructed using the giant colors pooled from the literature and the work of Blanco, McCarthy, and Blanco (1984) as a guide. Contamination from dwarfs, supergiants, and foreground disk giants is negligible ($\leq 3\%$). The M giant population is put together using the relative numbers of M6, M6.5, M7, M8, and M9 giants in Blanco *et al.* and adding a component of M1–M5 giants. Blanco does not give the relative numbers of early- to late-type giants because of incompleteness for the earlier types, but he does note that the early types probably outnumber the later types. Three cases will be calculated: case I where $n(\text{M1–M5}) = n(\text{M6–M9})$, corresponding to a high abundance of the latest types; case II, where $n(\text{M1–M5})/n(\text{M6–M9}) = 2$, which is probably close to the relative numbers in Baade's Window; and case III, where $n(\text{M1–M5})/n(\text{M6–M9}) = 3.3$ corresponding to the relative absolute space densities determined in the solar neighborhood (Mikami and Ishida 1981). The relative optical (V band) luminosities of the different components are adopted from Blanco *et al.* for the late types and Mikami and Ishida for the early types. The mean flux ratios for M1–M5 giants are calculated using M2–M3 standard stars from the Caltech list (see § IVd). Mean values of S_K/S_V and S_N/S_V as a function of spectral type are taken from the literature. These ratios are combined with the mean V flux to get the percentage of K ($2.2 \mu\text{m}$) and N ($10.2 \mu\text{m}$) flux in the population.

The M giant population synthesis is listed in Table 5. The flux-weighted percentages in the V , K , and N bands are given for the cases previously described. Three separate sets of mean flux ratios show the effect of truncating the giant branch at the very latest types. In general, the elliptical flux ratios are bluer than the model flux ratios, so earlier K giants must be added to make the synthesis complete. However, the importance of the latest M giants to the mean flux ratios is demonstrated clearly in Table 5. About one-third of the $10 \mu\text{m}$ flux is coming from the last two M subclasses, and removing them changes the

value of S_N/S_L by nearly a factor of 2. As a specific example, consider the reddest long-period variable in Baade's Window (D-11) studied by Jones, Hyland, and Robinson (1984). A component of such stars in ellipticals capable of reddening the $1\text{--}2 \mu\text{m}$ colors by only 3% would double the $10 \mu\text{m}$ flux. Therefore, the mid-infrared colors of these elliptical galaxies are very sensitive to the proportion of cool and luminous giants in the stellar population.

iii) Limits on Luminous Stars

Cool and luminous evolved stars can evidently produce most of the observed $10 \mu\text{m}$ flux from elliptical galaxies. The great majority of these stars are long-period variables ($\tau = 100\text{--}500$ days). They are of interest because they may be on the asymptotic giant branch (AGB), and the existence of massive and youthful stars in ellipticals is a matter of hot debate (Frogel and Whitford 1982; Wood and Bessell 1983; Jones, Hyland, and Robinson 1984). Regardless of the evolutionary phase of very cool stars, we can put constraints on their numbers based on their $1\text{--}4 \mu\text{m}$ colors. Since they have cooler effective temperatures than giants, long-period variables on the AGB can be isolated using near-infrared colors. We use flux ratios instead, since they make determining the relative numbers of different components more straightforward. Figure 9 shows the near-infrared flux ratios for the ellipticals, along with sequences of mean flux ratios for the giant-branch and long-period variables on the AGB. Giant flux ratios are taken from Frogel *et al.* (1978), with an extension to the latest spectral types from Dyck, Lockwood, and Capps (1974). Flux ratios for the long-period variables as a function of period are taken from the work by Wood and Bessel (1983) on Baade's Window. The flux ratios for the longest periods are based on small numbers of stars and are correspondingly uncertain.

The detectability of AGB stars from near-infrared data has been demonstrated by Persson *et al.* (1983) in LMC star clus-

TABLE 5
POPULATION SYNTHESIS: BAADE'S WINDOW M GIANTS
A.

TYPE (1)	S_K/S_L (2)	S_N/S_L (3)	CASE I ^a				CASE II ^b				CASE III ^c			
			n (%) (4)	S_V (%) (5)	S_K (%) (6)	S_N (%) (7)	n (%) (8)	S_V (%) (9)	S_K (%) (10)	S_N (%) (11)	n (%) (12)	S_V (%) (13)	S_K (%) (14)	S_N (%) (15)
M1–M5	2.10	0.14	50	74	8	2	67	85	25	8	77	91	45	29
M6	1.32	0.43	20	12	25	25	13	7	20	27	9	4	14	19
M6.5	1.36	0.40	17	8	32	26	11	5	25	23	8	3	18	16
M7	1.48	0.36	10	4	22	15	7	2	17	14	4	2	10	8
M8	1.12	0.79	2	1	6	11	1	~1	4	7	1	<1	4	7
M9	0.92	1.38	1	<1	7	21	~1	<1	9	21	~1	≤1	9	21
Elliptical	1.82	0.26

B.

Ratio	Set	Case I	Case II	Case III
$\langle S_K/S_L \rangle$	(M1–M9)	1.39	1.52	1.65
$\langle S_N/S_L \rangle$		0.65	0.61	0.56
$\langle S_K/S_L \rangle$	(M1–M8)	1.42	1.57	1.72
$\langle S_N/S_L \rangle$		0.45	0.41	0.34
$\langle S_K/S_K \rangle$	(M1–M7)	1.45	1.59	1.75
$\langle S_N/S_L \rangle$		0.39	0.37	0.30

^a Assumes giant branch with $n(\text{M1–M5}) = n(\text{M6–M9})$.

^b Assumes giant branch with $n(\text{M1–M5}) = 2n(\text{M6–M9})$.

^c Assumes giant branch with $n(\text{M1–M5}) = 3.3n(\text{M6–M9})$.

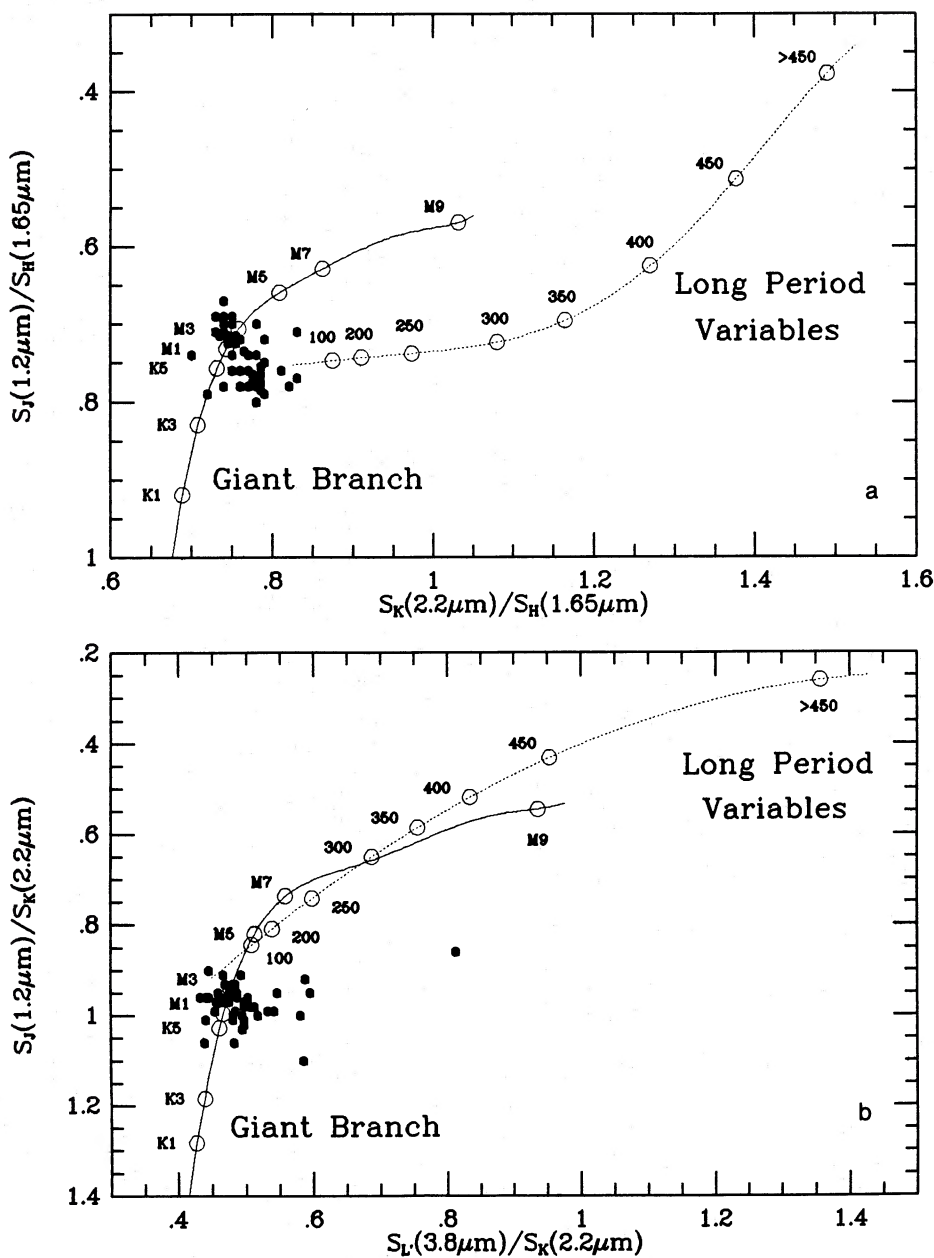


FIG. 9.—(a) Near-infrared flux ratios S_J/S_H vs. S_K/S_H for the elliptical galaxies. Also shown are mean flux ratios for giants as a function of spectral type and for long-period variables as a function of period in days. (b) As above, with infrared flux ratios S_J/S_K vs. S_L/S_K .

ters. While most clusters have $J-K \approx 0.60$, the intermediate age clusters (1–8 Gyr) often have very red colors of $J-K \approx 0.90-1.20$. The redness is due to carbon stars on the AGB which produce half the bolometric luminosity and a negligible portion of the visible light in the clusters. We do not have the CO indices for ellipticals which would allow us to identify carbon stars in ellipticals, but we note that late-type oxygen rich stars can give equally red $J-K$ colors. The elliptical galaxies in Figure 9 lie close to the track of giant-branch flux ratios, and the small scatter of the data puts a limit on the number of luminous long-period variables. Taking 300 days as the median of the period distribution, the corresponding luminosity is $M_{\text{bol}} = -4.5$ or well above the giant-branch tip (Wood and Bessel 1983). In Figure 9a, less than 15% of the 1–2 μm radiation can be coming from these AGB stars; other-

wise a 1σ redward shift in the mean ratio S_K/S_H would be detected due to the cooler photospheres of the AGB stars. The relative absolute 2.2 μm luminosities of the two components are $M_K = -5.1$ for M1 giants and $M_K = -7.4$ for 300 day variables. The limit on the relative numbers is therefore $n(\text{M1})/n(\text{AGB}) > 55$.

iv) Late Stages of Stellar Evolution in Ellipticals

It is important to place the M giants in the context of a realistic stellar population, since other late stages of evolution may generate infrared power. Renzini (1981) has calculated the colors and components of a coeval stellar population on the basis of a *stellar pipeline* picture. In this picture the relevant parameter is $b = N_{\text{PMS}}/t_{\text{PMS}}$, the ratio of the number of stars in a given post-main-sequence phase at any time to the time

TABLE 6
GALAXY POPULATION SYNTHESIS

EVOLUTIONARY PHASE		t^a (Myr)	M_{bol} (4)	M_K (5)	$V-K$ (6)	n (%) (7)	\dot{M}^b ($M_{\odot} \text{ yr}^{-1}$) (8)
(1)	(2)	(3)	(4)	(5)	(6)	(7)	(8)
Main sequence	(MS)	104	+7.60	...	2.7	65	...
Subgiant branch giants	(SGB)	10 ³	+4.50	...	2.2	5	...
	G8	730	+2.50	+0.55	2.2	20	<10 ⁻⁹
	K1	144	-0.75	-1.60	2.5	5	<10 ⁻⁹
	K3	14	-1.00	-3.32	2.9	2	<10 ⁻⁹
	K5	7.5	-1.50	-4.03	3.7	0.07	2 × 10 ⁻⁹
	M1	2.2	-2.50	-5.20	3.9	0.06	4 × 10 ⁻⁹
	M3	1.0	-3.50	-6.17	4.6	0.06	~10 ⁻⁸
	M5	0.21	-4.75	-7.59	6.2	0.01	~10 ⁻⁷
	M7	0.32	-5.50	-8.50	8.0	<0.01	~10 ⁻⁶
Horizontal branch	(HB)	100	-3.00	...	5.0	3	...
Asymptotic giants	(AGB)	~0.2	-5.00	0.03	~10 ⁻⁶

^a Giant luminosity function from Gun *et al.* 1981.

^b Mass-loss rates assume Reimers 1975 relationship.

spent in that phase. Essentially, b represents the flux of stars along an evolutionary sequence. The key quantity for galaxy synthesis in this model is not the *time* spent in a given evolutionary phase, but the *total energy released*. A substantial contribution to the infrared energy can be made by short-lived but luminous evolutionary phases.

Table 6 presents the synthesis for a 10 Gyr population with $Y = 0.22$ (Renzini 1981). Columns (1) and (2) show the evolutionary phase, and the dominance of the giants (51%) is clear. Columns (3), (4), and (5) have the lifetime, bolometric luminosity and absolute K magnitude, and the $V-K$ color of each phase is in column (6). These numbers come from the empirical old disk giant luminosity function (Tinsley and Gunn 1976, modified by Gunn, Stryker, and Tinsley 1981). The bolometric correction to the K magnitude ($M_{\text{bol}} = K_0 + \text{BC}_K$) comes from Frogel, Persson, and Cohen (1980) with an extension to redder colors by Wood and Bessell (1983). The same bolometric correction applies to both variables and nonvariables. Column (7) has the percentage of stars by number in each phase. Finally, estimates of the mass-loss rates for each type are listed in column (8). For early M types these numbers come from spectroscopic data collected in Reimers (1974), and for the important late M types the mass-loss rates come from the Reimers relation $\dot{M} (M_{\odot} \text{ yr}^{-1}) \approx 4 \times 10^{-13} L_{\odot} G_{\odot}/R_{\odot}$ and the empirical relation between $L_{\odot} g_{\odot}/R_{\odot}$ and infrared excess (i.e., S_N/S_L). These rates may be uncertain by a factor of 2–3, and Reimers (1974) has stressed the assumptions that are involved in estimating mass loss from infrared excess (the dust shell models are still quite simple, and the gas-to-dust ratios, expansion velocities, and optical depths at 10 μm are not well known for many stars). For AGB stars, the mass-loss rate for an initial mass of $\sim 1 M_{\odot}$ is given by Iben and Renzini (1983). Mass loss for the horizontal branch and earlier subluminescent phases can be ignored. The mass loss rates for the giants alone cover a factor of nearly 10⁴.

One conclusion from Table 6 is that the 10 μm flux must be produced from a tiny fraction of the stars in the galaxy population. The fraction of post-main-sequence stars is derived from Renzini (1981), using the flux $b = 1.4 \times 10^{-10}$ for a turnoff mass of 0.9 M_{\odot} . The time for post-main-sequence evolution goes as $t_{\text{PMS}} \approx 1.7 \times 10^9 M^{-2.72}$ from Sweigart and

Gross (1978), and 31% of the stars are PMS. The subdivisions of giants are taken from the space densities of old disk stars (Mikami and Ishida 1981; Reimers 1974), with an adjustment of the late M types to accord with the population in Baade's Window. Roughly 0.05% of the stellar population is contributing substantially to the 10 μm flux. The fraction is small enough that the completeness of the galaxy observations to all phases of evolution must be tested. From Renzini (1981), the number of stars in a given evolutionary phase is given by $n = 1.7 \times 10^{-11} M_{\text{tot}} t$. With $M/L \approx 15$ and half the galaxy light in a 6" aperture, the sample will have 1% fluctuations (10⁴ stars) for the shortest late M giant phases. Sampling statistics will therefore not affect the 10 μm fluxes. However, the luminosity function for the latest M types *cannot* be determined from disk stars in the solar neighborhood. To find 100 M7–M9 giants given a local star density of 0.1 pc⁻³ would require a search of 10¹⁰ pc³. Gunn, Stryker, and Tinsley (1981) had only two stars in the M5 bin of their local luminosity function. The latest M giants cannot be adequately represented in a locally defined sample.

Finally, the proposed population in Table 6 can be used to calculate the integrated mass loss over the nuclear regions of the ellipticals. The mass loss, like the infrared excess, is dominated by the short-lived but active stages of the luminous giants. The weighted mean mass-loss rate is $\approx 10^{-9} M_{\odot} \text{ star}^{-1} \text{ yr}^{-1}$ for the giants, and over 90% of this comes from the latest M types and AGB stars. The canonical number for gas shed by dying stars in ellipticals was calculated by Faber and Gallagher (1976) as $2 \times 10^{-10} M_{\odot} \text{ star}^{-1} \text{ yr}^{-1}$ for $M/L \approx 15$. This number is surprisingly resilient, changing little for different assumptions about the initial mass function (J. R. Mould, private communication). This mass loss rate leads to uncomfortable conflicts with the H I limits in times of only 10⁸ yr (Faber and Gallagher 1976; Knapp, Kerr, and Williams 1978). If the interpretation of the 10 μm excess as luminous late giants is correct, then we have directly observed the population responsible for most of the mass loss. Therefore, the actual mass-loss rate cannot be much lower than calculated in ellipticals. The ejected material is possibly being reprocessed into low-mass stars (Forman, Jones, and Tucker 1985). If it is not, an efficient gas and dust removal mechanism must be found.

VI. CONCLUSIONS

A large amount of new infrared data on the nuclei of elliptical galaxies has been collected. In particular, this is the first large set of data at $10\ \mu\text{m}$ where the presence of cool stellar components and weak nonthermal components can be tested. The principal result of the $10\ \mu\text{m}$ survey is the discovery of a component in 30% of the sample that cannot be attributed to photospheric emission from the late-type giant population. The statistical significance of this weak excess has been confirmed with a variety of nonparametric statistical tests. The following conclusions are drawn from the infrared survey:

1. About 30% of the sample show a significant excess over photospheric emission at $10\ \mu\text{m}$, and the galaxies with strong $10\ \mu\text{m}$ emission are not distinctive in terms of their optical properties. For example, excess $10\ \mu\text{m}$ emission is not necessarily associated with the mass or luminosity of the galaxy, or with the presence of a nuclear dust lane or a weak disk component. The strong ellipticals typically have $\sim 5\%$ of the $10\ \mu\text{m}$ luminosity of NGC 1052.
2. We have made multiaperture measurements of M32 at $2\ \mu\text{m}$ and $10\ \mu\text{m}$ and find a similar excess over giant photospheric emission. In M32, the excess $10\ \mu\text{m}$ emission follows the spatial distribution of the stars seen at $2\ \mu\text{m}$.
3. The infrared excess in ellipticals is steep, with an equivalent color temperature of $T_c \leq 700\ \text{K}$, although a weak power-law component would also reproduce the $1\text{--}10\ \mu\text{m}$ colors. Only when the excess is very strong is it noticeable in the *JHKL* data. The $1\text{--}4\ \mu\text{m}$ colors are very homogeneous, and a spread of only one or two giant subclasses is needed to encompass most of the galaxies. Internal reddening in ellipticals must be less than 0.3 visual mag on average.
4. The color gradient found by Frogel *et al.* (1978) is confirmed with this smaller aperture data. Galaxy *J-K* colors become noticeably redder towards the center in this sample. If the color gradient is caused by a metallicity effect, then the centers of ellipticals have abundances at least twice the solar value.
5. Excess radiation at $10\ \mu\text{m}$ can be generated by weak non-thermal power laws resulting from nuclear activity. The infrared power law derived from the $10\ \mu\text{m}$ and *IRAS* data for these galaxies are systematically steeper than power laws seen in quasars. However, there is only weak evidence against the existence of miniblazars in the cores of some ellipticals, and it is difficult to rule out copious but low-luminosity analogs of the radio-quiet quasars, since the optical/infrared and radio fluxes are not expected to be correlated.
6. Strong infrared emission from hot dust associated with active star-forming regions is effectively ruled out in these galaxies, with the possible exception of NGC 838. If heated dust is

reradiating in the infrared, it must be in the form of circumstellar shells rather than diffuse dust distributed between the stars.

7. A good match to the $1\text{--}10\ \mu\text{m}$ colors is obtained by assuming that the infrared light comes from late-type giants with the same luminosity function as observed in the galactic nuclear bulge. The M giant $10\ \mu\text{m}$ luminosity function is calculated from data for local M giants in the literature. As has been observed in Baade's Window, late M giants are likely to be an important component in elliptical galaxy models. The late M giants which provide one-third of the $10\ \mu\text{m}$ flux make a negligible contribution in the optical.

8. A majority of the excess $10\ \mu\text{m}$ radiation over photospheric emission in ellipticals plausibly comes from cool and luminous stars with $M_{\text{bol}} < -3.6$, i.e., stars with an excess due to dust from mass loss on the asymptotic giant branch. This is consistent with the observation in M32 that the excess $10\ \mu\text{m}$ emission follows the spatial distribution of the stars. The small dispersion in near-infrared colors allows an upper limit of $\sim 15\%$ to be put on the fraction of $1\text{--}2\ \mu\text{m}$ radiation coming from AGB stars, because the presence of stars with cooler photospheres would produce a shift in the near-infrared colors.

9. In terms of galaxy evolution, it appears that most of the $10\ \mu\text{m}$ radiation is coming from short-lived periods ($\leq 10^6\ \text{yr}$) of high mass loss ($\sim 10^{-6}\ M_{\odot}\ \text{yr}^{-1}$) in the late phases of giant evolution. These stars have previously been neglected because of their weak optical flux. The observation of this high mass-loss component in elliptical galaxies means that the conflict between the expected products of stellar evolution and the low H I limits cannot be resolved by invoking a lower mass-loss rate.

We would like to thank Ron Koehler, Charlie Kaminski, Dave Greip, and John Hamilton for their nights of careful support on the IRTF. We are also grateful to Dolores Walther for assistance on the UKIRT and to the staff of the VLA for help with the radio observations. Jim Heasley provided the algorithm for the Lucy method, and John Peacock provided useful suggestions on statistical tests. Nick Scoville and Nick Devereux kindly allowed us to use data on NGC 4550 and NGC 4880 before publication. We thank John Tonry for the MONGO plottage package. We acknowledge lively discussions with Greg Bothun, Jay Frogel, Jeremy Mould, Jim Rose, and John Tonry. An anonymous referee considerably helped the presentation of this paper. C. D. I. is grateful for support provided by the SERC under a NATO Fellowship at the Institute for Astronomy, Hawaii, and part of this work was carried out under a Caltech Weingart Fellowship. E. E. B. and C. G. W.-W. were supported under NSF grants AST 82-17118 and AST 84-18197.

REFERENCES

- Aaronson, M. 1981, *IAU Symposium 96, Infrared Astronomy*, ed. C. G. Wynn-Williams and D. P. Cruikshank (Dordrecht: Reidel), p. 297.
- Aaronson, M., Cohen, M., Mould, J., and Malkan, M. 1978, *Ap. J.*, **223**, 824.
- Allen, D. A., and Cragg, T. A. 1982, *M.N.R.A.S.*, **203**, 777.
- Balick, B., and Heckman, T. 1983, *Ann. Rev. Astr. Ap.*, **20**, 431.
- Becklin, E., Tokunaga, A., and Wynn-Williams, C. G. 1982, *Ap. J.*, **263**, 624.
- Bertola, F., and Oke, J. B. 1982, in *Third European IUE Conference*, ed. E. Rolfe, A. Heck, and B. Batrick (Noordwijk, The Netherlands: ESA), p. 151.
- Blanco, B. M., Blanco, V. M., and McCarthy, M. F., S. J. 1978, *Nature*, **271**, 639.
- Blanco, V. M., McCarthy, M. F., S. J. and Blanco, B. M. 1984, *A.J.*, **89**, 636.
- Burstein, D., and Heiles, C. 1982, *A.J.*, **87**, 1165.
- Burstein, D., Faber, S., Gaskell, C. M., and Krumm, N. 1984, *Ap. J.*, **287**, 586.
- Coleman, G., Wu, C.-C., and Weedman, D. 1980, *Ap. J. Suppl.*, **43**, 393.
- Condon, J., O'Dell, S., Puschell, J., and Stein, W. 1981, *Ap. J.*, **246**, 624.
- Cruz-Gonzales, I., and Huchra, J. P. 1984, *A.J.*, **89**, 441.
- Davies, R. L., Efstathiou, G., Illingworth, G., and Schechter, P. L. 1983, *Ap. J.*, **266**, 41.
- Davies, R. L., and Illingworth, G. 1983, *Ap. J.*, **266**, 516.
- de Jong, T., *et al.* 1984, *Ap. J. (Letters)*, **278**, L69.
- de Vaucouleurs, G., de Vaucouleurs, A., and Corwin, H. G., Jr. 1976, *Second Reference Catalog of Bright Galaxies* (Austin: University of Texas Press) (RC2).
- Disney, M. J., and Wall, J. V. 1977, *M.N.R.A.S.*, **179**, 235.
- Dressel, L. L., and Condon, J. J. 1978, *Ap. J. Suppl.*, **36**, 53.
- Dyck, H. M., Lockwood, G. W., and Capps, R. W. 1974, *Ap. J.*, **189**, 89.
- Elias, J. A., Frogel, J. A., Matthews, K., and Neugebauer, G. 1982, *A.J.*, **87**, 1029.
- Faber, S. M., and Gallagher, J. S. 1976, *Ap. J.*, **204**, 365.

- Forman, W., Jones, C., and Tucker, W. 1985, *Ap. J.*, **293**, 102.
 Frogel, J. A., Cohen, J. G., and Persson, S. E. 1983, *Ap. J.*, **275**, 773.
 Frogel, J. A., Persson, S. E., Aaronson, M., Becklin, E. E., Matthews, K., and Neugebauer, G. 1975, *Ap. J. (Letters)*, **195**, L15.
 Frogel, J. A., Persson, S. E., Aaronson, M., and Matthews, K. 1978, *Ap. J.*, **220**, 75.
 Frogel, J. A., Persson, S. E., and Cohen, J. G. 1980, *Ap. J.*, **240**, 785.
 Frogel, J. A., and Whitford, A. E. 1982, *Ap. J. (Letters)*, **259**, L7.
 Frogel, J. A., Whitford, A. E., and Rich, R. M. 1984, *A.J.*, **89**, 1536.
 Gunn, J. E., Stryker, L. L., and Tinsley, B. M. 1981, *Ap. J.*, **249**, 48.
 Habing, H. J., et al. 1984, *Ap. J. (Letters)*, **278**, L59.
 Hagen, W. 1978, *Ap. J. Suppl.*, **38**, 1.
 Heckman, T. M., Lebofsky, M. J., Rieke, G. H., and van Breugel, W. 1983, *Ap. J.*, **275**, 61.
 Hummel, E. 1980, *Astr. Ap. Suppl.*, **41**, 151.
 Hummel, E., Kotanyi, C. G., and Ekers, R. D. 1986, *Astr. Ap.*, in press.
 Iben, I., Jr., and Renzini, A. 1983, *Ann. Rev. Astr. Ap.*, **21**, 271.
 Impey, C. D., Brand, P. W. J. L., Williams, P. M., and Wolstencroft, R. D. 1984, *M.N.R.A.S.*, **209**, 245.
 Impey, C. D., Wynn-Williams, C. G., and Becklin, E. E. 1986, in preparation (Paper II).
 Jedrzejewski, R. I. 1985, Ph.D. thesis, University of Cambridge.
 Jones, T. J., Hyland, A. R., and Robinson, G. 1984, *A.J.*, **89**, 999.
 Knapp, G. R., Kerr, F. J., and Williams, B. A. 1978, *Ap. J.*, **222**, 800.
 Knapp, G. R., Turner, E. L., and Cunniffe, P. E. 1985, *A.J.*, **90**, 454.
 Koornneef, J. 1983, *Astr. Ap. Suppl.*, **45**, 5.
 ———. 1984, *Astr. Ap.*, **51**, 500.
 Kurucz, R. L. 1979, *Ap. J. Suppl.*, **40**, 1.
 Lilly, S. J., and Longair, M. S. 1982, **199**, 1053.
 Lloyd Evans, T. 1976, *M.N.R.A.S.*, **174**, 169.
 Lucy, L. B. 1974, *A.J.*, **79**, 745.
 Meier, D., Ulrich, M.-H., Fanti, R., Gioia, I., and Lari, C. 1979, *Ap. J.*, **229**, 25.
 Mikami, T., and Ishida, K. 1981, *Pub. Astr. Soc. Japan*, **33**, 135.
 Neugebauer, G., Oke, J. B., Becklin, E., and Matthews, K. 1979, *Ap. J.*, **230**, 79.
 Neugebauer, G., Soifer, B., Rice, W., and Rowan-Robinson, M. 1984, *Pub. A.S.P.*, **96**, 973.
 O'Connell, R. W. 1976, *Ap. J.*, **206**, 370.
 ———. 1980, *Ap. J.*, **236**, 430.
 O'Dell, S. L., Puschell, J. J., Stein, W. A., and Warner, J. W. *Ap. J. Suppl.*, **38**, 267.
 Persson, S. E., Aaronson, M., Cohen, J. G., Frogel, J. A., and Matthews, K. 1983, *Ap. J.*, **266**, 105.
 Persson, S. E., Frogel, J. A., and Aaronson, M. 1979, *Ap. J. Suppl.*, **39**, 61.
 Puschell, J. J. 1981a, *Ap. J.*, **247**, 48.
 ———. 1981b, *A.J.*, **86**, 16.
 Reimers, D. 1974, in *Problems in Stellar Atmospheres and Envelopes*, ed. B. Baschek, W. Kegel, and G. Traving (Berlin: Springer), p. 229.
 ———. 1975, *Mém. Soc. Roy. Sci. Liège, 6e Sér.*, **8**, 369.
 Renzini, A. 1977, in *Advanced Stages in Stellar Evolution*, ed. I. Iben, Jr., A. Renzini, and D. Schramm (Geneva: Geneva Observatory), p. 151.
 ———. 1981, *Ann. de Phys.*, **6**, 87.
 Rieke, G. H. 1978, *Ap. J.*, **226**, 550.
 Rieke, G. H., and Lebofsky, M. J. 1978, *Ap. J. (Letters)*, **220**, L38.
 Rieke, G. H., Lebofsky, M. J., and Kemp, J. C. 1982, *Ap. J. (Letters)*, **252**, L53.
 Rieke, G. H., and Low, F. J. 1972, *Ap. J. (Letters)*, **176**, L95.
 Rose, J. A. 1985, *A.J.*, **90**, 1927.
 Rose, J. A., and Tripicco, M. J. 1984, *Ap. J.*, **285**, 55.
 Rowan-Robinson, M., et al. 1984, *Ap. J. (Letters)*, **278**, L7.
 Ryster, C., and Puget, J. L. 1977, *Ap. J.*, **215**, 775.
 Sadler, E. M., and Gerhard, O. E. 1985, *M.N.R.A.S.*, **214**, 177.
 Sandage, A. R., and Tammann, G. A. 1981, *A Revised Shapley-Ames Catalog of Bright Galaxies* (Washington: Carnegie Institution of Washington).
 Schechter, P. L., and Gunn, J. E. 1979, *Ap. J.*, **229**, 472.
 Schwartz, D. A., and Ku, W. H.-M. 1983, *Ap. J.*, **266**, 459.
 Schweizer, F. 1979, *Ap. J.*, **233**, 23.
 Scoville, N. Z., Becklin, E. E., Young, J. S., and Capps, R. W. 1983, *Ap. J.*, **271**, 512.
 Sellgren, K. 1984, *Ap. J.*, **277**, 623.
 Siegel, S. 1956, *Nonparametric Statistics for the Behavioral Sciences* (New York: McGraw-Hill), p. 116.
 Stebbins, J., and Whitford, A. E. 1948, *Ap. J.*, **108**, 413.
 Sweigart, A. V., and Gross, P. G. 1978, *Ap. J. Suppl.*, **36**, 406.
 Tinsley, B. M. 1972, *Ap. J.*, **178**, 319.
 ———. 1978, *Ap. J.*, **222**, 14.
 Tinsley, B. M., and Gunn, J. E. 1976, *Ap. J.*, **203**, 52.
 Tonry, J. L. 1984, *Ap. J. (Letters)*, **283**, L27.
 Tonry, J. L., and Davis, M. 1981, *Ap. J.*, **246**, 666.
 van den Bergh, S. 1975, *Ann. Rev. Astr. Ap.*, **13**, 217.
 Whitford, A. E. 1976, in *Stars and Stellar Systems, Vol. 9, Galaxies and the Universe*, ed. A. Sandage, M. Sandage, and J. Kristian (Chicago: University of Chicago Press), p. 159.
 Wood, P. R., and Bessel, M. S. 1983, *Ap. J.*, **265**, 748.
 Wrobel, J. M. 1986, *A.J.*, in press.
 Wynn-Williams, C. G., and Becklin, E. E. 1984, *Ap. J.*, **290**, 108.

E. E. BECKLIN and C. G. WYNN-WILLIAMS: Institute for Astronomy, 2680 Woodlawn Drive, Honolulu, HI 96822

CHRIS IMPEY: 105-24 Robinson, California Institute of Technology, Pasadena, CA 91125